Department of Applied Physics

Role of hydrogenic molecules in fusion–relevant divertor plasmas

Andreas Holm

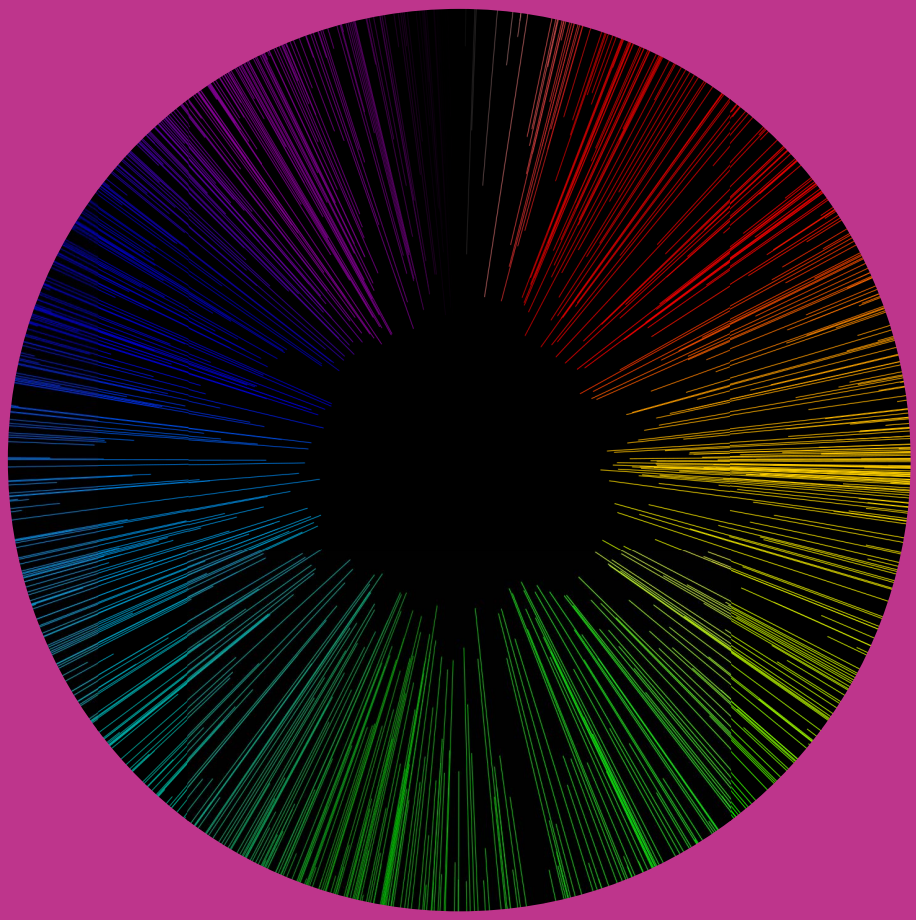

Aalto University

DOCTORAL THESES

Aalto University publication series
DOCTORAL THESES 106/2022

Role of hydrogenic molecules in fusion-relevant divertor plasmas

Andreas Holm

A doctoral thesis completed for the degree of Doctor of Science (Technology) to be defended, with the permission of the Aalto University School of Science, at a public examination held at the lecture hall M1 of the Undergraduate Center (Otakaari 1) at noon, September 9th 2022.

Aalto University
School of Science
Department of Applied Physics
Fusion and Plasma Physics

Supervising professor
Professor Mathias Groth, Aalto University, Finland

Thesis advisor
Professor Mathias Groth, Aalto University, Finland

Preliminary examiners
Daren Stotler, Princeton Plasma Physics Laboratory, United States of America
David Coster, Max-Planck-Institut für Plasmaphysik, Germany

Opponent
Professor Ursel Fantz, Max-Planck-Institut für Plasmaphysik, Germany

Aalto University publication series
DOCTORAL THESES 106/2022

ISBN 978-952-64-0889-7 (printed)
ISBN 978-952-64-0890-3 (pdf)
ISSN 1799-4934 (printed)
ISSN 1799-4942 (pdf)
http://urn.fi/URN:ISBN:978-952-64-0890-3

Images: Andreas Holm

Unigrafia Oy
Helsinki 2022

Finland

Publication orders (printed book):
andreas.holm@aalto.fi

NORDIC SWAN ECOLABEL
Printed matter
4041-0619

Aalto University

Abstract

Aalto University, P.O. Box 11000, FI-00076 Aalto www.aalto.fi

Author
Andreas Holm

Name of the doctoral thesis
Role of hydrogenic molecules in fusion-relevant divertor plasmas

Publisher School of Science

Unit Department of Applied Physics

Series Aalto University publication series DOCTORAL THESES 106/2022

Field of research Fusion and Plasma Physics

Manuscript submitted 1 April 2022 **Date of the defence** 9 September 2022

Permission for public defence granted (date) 20 June 2022 **Language** English

☐ **Monograph** ☒ **Article thesis** ☐ **Essay thesis**

Abstract

Power production using magnetic confinement fusion is technically challenging and necessitates operation under detached divertor conditions. Under detached conditions the power loads to the plasma-facing components are reduced within their thermo-mechanical properties. Molecular processes are critical at temperatures relevant to onset of plasma detachment. Therefore, molecules are expected to affect the local plasma conditions and the onset of detachment. This dissertation evaluates the role of molecular effects on the onset of detachment using a fluid model for molecules implemented in the edge-fluid code UEDGE coupled to the collisional-radiative (CR) code CRUMPET. The applicability of the molecular fluid model is assessed using the kinetic neutral Monte-Carlo code EIRENE. To assess the validity of the predictions, and to quantify the role of molecular particle and power sinks on the onset of detachment, the numerical UEDGE predictions are compared to Divertor Thomson Scattering (DTS) and Langmuir probe measurements in DIII–D low-confinement (L-mode) plasmas.

Including fluid molecules in UEDGE simulations of deuterium plasmas in L-mode conditions improves the qualitative code-experiment agreement for detachment onset compared to UEDGE simulations considering atoms only. Accounting for molecularly-induced plasma particle and power sinks in the simulations reduces the plasma temperatures sufficiently for detachment onset to occur. The role of electronic and vibrational CR transitions are shown to be more important for the effective CR dissociation rates than the assumption of ion-electron thermal equilibration and non-local transport effect of vibrationally excited molecules. Omitting vibrational and electronic transitions from EIRENE simulations decrease effective dissociation rates by up to 65% compared to when they are included.

UEDGE fluid predictions of molecular content and mean energy are shown to lie within 15% and a factor of 2 of EIRENE kinetic predictions, respectively. These findings indicate that a fluid treatment of the molecules in divertor plasmas is applicable for divertor-relevant conditions. Using fluid molecular models in plasma-edge simulations reduces the computational times compared to kinetic molecular models, especially under highly collisional conditions encountered in detached divertor plasmas. The effect of approximating the molecules as a fluid is found to be smaller than that of other processes affecting molecular predictions, such as the CR processes included in the effective rates. The dissertation suggests a number of improvements to the implemented molecular fluid model to further reduce the difference between kinetic and fluid molecular models.

Keywords plasma physics, fusion, detachment, molecules, collisional-radiative model

ISBN (printed) 978-952-64-0889-7 **ISBN (pdf)** 978-952-64-0890-3

ISSN (printed) 1799-4934 **ISSN (pdf)** 1799-4942

Location of publisher Helsinki **Location of printing** Helsinki **Year** 2022

Pages 130 **urn** http://urn.fi/URN:ISBN:978-952-64-0890-3

Författare
Andreas Holm

Doktorsavhandlingens titel
Role of hydrogenic molecules in fusion-relevant divertor plasmas

Utgivare Högskolan för teknikvetenskaper

Enhet Högskolan för Teknikvetenskaper

Seriens namn Aalto University publication series DOCTORAL THESES 106/2022

Forskningsområde Fusion och Plasmafysik

Inlämningsdatum för manuskript 01.04.2022 **Datum för disputation** 09.09.2022

Beviljande av disputationstillstånd (datum) 20.06.2022 **Språk** Engelska

☐ **Monografi** ☒ **Artikelavhandling** ☐ **Essäavhandling**

Sammandrag

Energiproduktion med magnetisk inneslutningsfusion är tekniskt utmanande och förutsätter frigjorda (*detached*, egen övers.) plasma för att sänka effekten som når de plasmautsatta komponenterna till acceptabla nivåer. Molekylära processer är relevanta vid temperaturer associerade med plasmats frigörning från reaktorns innervägg. Denna avhandling utvärderar de molekylära processernas roll i plasmats frigörning med hjälp av en molekylär vätskemodell som implementerats i plasmakoden UEDGE som kopplats till den kollisionsradiativa (*collisional-radiative*, CR, egen övers.) koden CRUMPET. Tillämpligheten av den molekylära vätskemodellen utvärderas med hjälp av den kinetiska koden EIRENE, som simulerar transport av neutrala partiklar. Validiteten av UEDGE-simuleringarna och molkylernas roll i plasmats frigörning utvärderas genom att jämföra förutsägelser för s.k. *L-mode* deuteriumplasma i tokamaken DIII–D med mätresultat från en s.k. Divertor Thomson-Scattering (DTS) spektrometer och från Langmuirsonder.

Den molekylära vätskemodellen förbättrar den kvalitativa jämförbarheten mellan UEDGE-simuleringar och DIII-D L-mode deuteriumexperiment jämfört med UEDGE-simuleringar som inte beaktar molekyler. Partikel- och energiförluster som orsakas av molekylära processer leder till en sänkning av plasmatemperaturen och plasmats frigörning i simuleringarna. Elektroniska och vibrationella övergångar påvisas ha en större inverkan på den effektiva CR-dissociationsraten än antagandet att plasmats elektroner och joner är i termisk jämnvikt eller icke-lokal transport av vibrationsexciterade molekyler. Den effektiva dissociationsraten minskade med 65% i EIRENE-simuleringar då elektroniska och vibrationella övergångar utelämnades jämfört med då de beakteades.

Förutsägelser av molekylernas antal och medelenergi i UEDGE-simuleringar med den molekylära vätskemodellen ligger inom 15% respektive en faktor 2 av förutsägelser av kinetiska EIRENE-simuleringar. Denna överrensstämmelse antyder att en molekylär vätskemodell kan vara tillämpbar för divertorrelevanta plasma. En vätskemodell för molekyler har kortare beräkningstid jämfört med kinetiska modeller för molekyler, säsrkilt i frigjorda plasma. Inverkan av att approximera molekylerna som en vätska är mindre än inverkan av andra processer som påverkar molekylära förutsägelser, exempevis vilka CR-processer som beaktas då de effektiva reaktionsraterna beräknas. Avhandlingen presenterar ett antal förbättringsförslag för den implementerade molekylära vätskemodellen för att ytterligare minska skillnaden mellan de kinetiska modellerna och de molekylära vätskemodellerna.

Nyckelord plasmafysik, fusion, plasmats frigörning, molekyler, kollisionsradiativ modell

ISBN (tryckt) 978-952-64-0889-7 **ISBN (pdf)** 978-952-64-0890-3

ISSN (tryckt) 1799-4934 **ISSN (pdf)** 1799-4942

Utgivningsort Helsingfors **Tryckort** Helsingfors **År** 2022

Sidantal 130 **urn** http://urn.fi/URN:ISBN:978-952-64-0890-3

Preface

Humanity is presently participating in a 100 m sprint against our previous obliviousness and, regrettably, subsequent negligence towards the delicate environmental equilibrium that has persevered on Earth through ages. Due to the nature of the competition, the start gun has already sounded, while we have been blissfully unaware of our involuntary participation in a race to escape oblivion. The first heads have started turning, wondering why there is no action. The first voices are raised from the stands, egging us to start moving. Meanwhile, we are staring down the back of our adversary, a good 20 m down the track, edging further away from us at an accelerating pace in each moment of inactivity and indecisiveness. These few meters of head start has already seen disastrous consequences in the form of numerous “once-in-a-lifetime” events during my lifetime: spiraling increases in global temperatures, shorter winters, record heatwaves, wildfires, and extreme weather, as well as a global pandemic, in addition to geopolitical tensions due to increasingly scarce resources. All of these adverse effects are related to man-made climate change and habitat-loss of wildlife due to industrial-scale deforestation.

We have, indeed, taken our first lurch - a few wobbly, trying steps - in the race by increasing renewable energy production and starting the sluggish transformation of our transportation sector towards electrical vehicles, which eventually will result in affordable and guilt-free mobility for the masses rather than for the fortunate few. However, we need to multiply our efforts by engaging the technological sector and all legislative power available to increase our fossil-free energy production by wind, solar, and fission to keep us in the race, within grasp of victory. Because, with the present public interest and funding in fusion technology, it seems increasingly likely that fusion will only spring our step - and make the distance to the finish line of no consequence - when the race is already all but lost. However, to my great pleasure, several foundations and organizations have recognized the prospects of fusion energy, and taken action by financially supporting this thesis. I would like to express my heartfelt gratitude to the following foundations and organizations for

their support: the Fulbright Finland Foundation, the Walter Ahlström Foundation, Svensk-Österbottniska Samfundet, Svenska Tekniska Vetenskapsakademien i Finland, the Foundation for Aalto University Science and Technology, the Waldemar von Frenckell Foundation, the Fortum Foundation, and Tekniska Föreningen i Finland.

Against this backdrop, I have pursued a doctoral degree within the field of fusion technology, in hope to contribute to a future with fair and sustainable energy production. Despite the global challenges, also affecting my doctoral project by the global COVID pandemic that stymied scientific progress by cancelling in-person international collaboration and conferences for over two years, I will be crossing the finish line of my doctoral degree, the culmination of studies started exactly ten years ago. During this time, I have been inspired by the passion and investment of previous generations of fusion researchers who have tirelessly advanced the field, many of whom I have had the honor to work with. Furthermore, I have been encouraged by the growing interest in fusion research by students whom I have had the pleasure of interacting with and in some cases teach and advise. These experiences instill me with hope that the work invested in fusion will come to fruition and benefit future generations before the damage to our planet becomes irreversible.

This doctoral thesis is not a personal achievement but, rather, a monument to all those who have supported me over the years, professionally and privately. I can scarcely thank all who have supported me by name in these few pages but I will, nevertheless, name some. First and foremost, I express my gratitude to Professor Mathias Groth and Tom Rognlien. Mathias supervised and advised my doctoral project and advised me since we first crossed paths while I applied for a summer internship in the fusion group in 2015. I am deeply grateful for the professional and academic opportunities, such as a Fulbright grant to LLNL, I have had while working for Mathias. Furthermore, I admire his diligence and attention to detail, as well as the time and effort Mathias invests in his advisees, epitomized by the 581 comments on the first draft of this thesis. Your mentorship was one of the key reasons I opted to pursue a doctoral degree within the field. I consider myself lucky to count you as my “Doktorvater” and friend. Tom acted as my academic advisor during my Fulbright grant to LLNL and has tirelessly taught me the inner workings of UEDGE and assisted me since 2016. Your friendliness made me feel at home when thousands of miles from home. I hope that, in time, I will possess even part of your eloquence, patience, and knowledge.

Furthermore, I would like to express my gratitude towards Steve Allen, Alex Friedman, and Harry McLean for their administrative and scientific support for my research visits, Fulbright application, and subsequent grant. I am incredibly grateful for the support and insights of my co-authors Bill Meyer, Petra Börner, and Dirk Wünderlich. I would also like to thank Adam

McLean, Detlev Reiter, George Wilkie, Eric Meier, and my colleagues at Aalto University for valuable scientific discussions throughout my doctoral studies. I am grateful for the valuable and insightful comments on this thesis by Darren Stotler and David Coster, who acted as pre-examiners. I am also directing a special thanks to Professor Urself Fantz for acting as opponent of my public examination. An honorable mention goes to the Aalto and PHYS floorball squads, that have offered an escape from desk work in the form of rigorous physical exercise. A special shout-out to the LLNL "Lunch Squad" that provided much needed comfort and social support during the early months of the 2020 COVID pandemic in the form of remote lunches, and subsequently served as a valuable contact to the US fusion program. I am looking forward to face-to-face lunches in the near future.

I am incredibly grateful for my peers, who provided the support necessary to persevere through my studies. During my first day at Aalto, I befriended a group of my closest friends, a posse aptly nicknamed "Superfysikerna". I am deeply grateful for all our long days and nights of studies for the excruciating "Laaja-mellisar" and numerous other courses and exams, without which I am certain that I would have faltered on numerous occasions. The stress and fatigue of the demanding studies have also been balanced by close involvement with Teknologföreningen, TF, where I still am continuously making new acquaintances. I am incredibly thankful for the camaraderie and opportunities TF has provided me with throughout my studies, providing well-earned breaks from academic woes. Despite my 2018 graduation, and subsequent alumnification, I have been unable to abstain from these activities amid the stress and intensity of my doctoral studies, which speaks volumes to the qualifications and importance of TF.

Finally, I want to express my deepest gratitude to my family. Without your encouragement and active engagement in my undertakings I would not have persevered. I am indebted to you, Sonja, for picking me up when at my lowest, supporting me throughout my work, and for all the cherished moments and memories we have experienced during the last few years. I would like to especially thank my grandparents, Eino and Helena, for your unwavering support and love over all these years. This thesis is dedicated to you. Utan er skulle jag aldrig ha uppnått allt jag uppnått. Tusen tack för allt ni gjort för mig och oss, och Heja Sport!

Espoo, August 9, 2022,

Andreas Holm

Contents

List of Publications

This thesis consists of an overview and of the following publications which are referred to in the text by their Roman numerals.

I A. Holm, P. Börner, T.D. Rognlien, W.H. Meyer, and M. Groth, "Comparison of a collisional-radiative fluid model of H_2 in UEDGE to the kinetic neutral code EIRENE", *Nuclear Materials and Energy* **27** (2021) 100982.

II A. Holm, T.D. Rognlien, and W.H. Meyer, "Implementation and assessment of an extended hydrogenic molecular model in UEDGE", *Contributions to Plasma Physics* **60** (2020) e201900150.

III A. Holm, M. Groth, and T.D. Rognlien, "Assessing ion–electron thermal equilibration in the scrape-off layer of tokamaks using UEDGE", *Contributions to Plasma Physics* **58** (2018) 547.

IV A. Holm, D. Wünderlich, M. Groth, and P. Börner, "Impact of vibrationally resolved H_2 on particle balance in Eirene simulations", *Contributions to Plasma Physics* (2022) e202100189.

V A. Holm, M. Groth, and T.D. Rognlien, "UEDGE-predicted impact of molecules on low-field side target detachment in DIII–D", *Nuclear Materials and Energy* **19** (2019) 143.

Authors' contributions

Publication I: "Comparison of a collisional-radiative fluid model of H_2 in UEDGE to the kinetic neutral code EIRENE"

The author implemented the collisional-radiative effective rates into the UEDGE fluid model. The author's contribution included the creation of the CRUMPET tool for calculating the relevant rates and formulation of the electron, ion-atom, binding energy, and radiative plasma effective collisional-radiative sink and source terms. The author performed and analyzed the numerical UEDGE and EIRENE simulations with the assistance of the co-authors. The author presented the results at a conference, authored the manuscript, and corresponded with the referees. P. Börner provided an example EIRENE case, verified modifications of the example case, and assisted with the necessary changes to the EIRENE simulations. T.D. Rognlien assisted with the changes to the UEDGE source code and provided academic supervision and counseling. W.H. Meyer provided support for the Python interfacing of UEDGE. M. Groth provided academic supervision and counseling.

Publication II: "Implementation and assessment of an extended hydrogenic molecular model in UEDGE"

The author performed the UEDGE simulations using the models created by the co-authors, analyzed the results, and verified the predictions against analytic solutions. The author presented the results at a workshop, authored the manuscript, and corresponded with the referees. T.D. Rognlien derived and implemented the molecular equations into the UEDGE source code and provided academic supervision and counseling. W.H. Meyer developed the Python interface for UEDGE and provided support for its use.

Publication III: "Assessing ion–electron thermal equilibration in the scrape-off layer of tokamaks using UEDGE"

The author formulated and applied the analytic model presented in the work. The author performed the UEDGE simulations prepared by the co-authors, analyzed the results, and compared them to the analytic model predictions. The author presented the results at a workshop, authored the manuscript, and corresponded with the referees. T.D. Rognlien assisted with the setup of the UEDGE simulations and supported the analysis of UEDGE predictions. M. Groth provided academic supervision and counseling.

Publication IV: "Impact of vibrationally resolved H_2 on particle balance in Eirene simulations"

The author prepared and performed the EIRENE and YACORA simulations and was responsible for comparing and interpreting the predictions. The author performed the EIRENE simulations, analyzed the results, and compared them to the analytic model predictions. The author presented the results at a workshop, authored the manuscript, and corresponded with the referees. D. Wünderlich verified the YACORA simulations and provided the "standard YACORA" results. M. Groth coordinated the collaboration and provided academic supervision and counseling. P. Börner assisted with modifications to the EIRENE simulations and verified their implementation.

Publication V: "UEDGE-predicted impact of molecules on low-field side target detachment in DIII–D"

The author performed the UEDGE simulations, post-processed the results, and conducted the comparison to experimental data. The author presented the results at a conference, authored the manuscript, and corresponded with the referees. M. Groth participated in the plasma experiments, analyzed and provided the experimental measurements, and provided academic supervision and counseling. T.D. Rognlien provided an example UEDGE case, assisted with the modifications of the simulations, and verified the changes made to the simulations.

1. Introduction

The lightest element, hydrogen, has been central in advancing the fields of atomic and molecular physics due to its simple structure of a single electron orbiting a proton. Furthermore, hydrogen may provide a means to meet the increasing global energy demand without release of harmful greenhouse gases or high-level radioactive waste by the principle of fusion. In fusion reactions the hydrogen isotopes deuterium (D) and tritium (T), with one and two nuclear neutrons (n) in addition to the proton (p), respectively, fuse into helium (He), releasing energy by the principle of mass-deficit:

$$^2\mathrm{D} + {}^2\mathrm{D} \rightarrow {}^3\mathrm{He} + \mathrm{n} \quad (3.3\ \mathrm{MeV}) \tag{1.1}$$

$$^2\mathrm{D} + {}^2\mathrm{D} \rightarrow {}^3\mathrm{T} + \mathrm{p} \quad (4.0\ \mathrm{MeV}) \tag{1.2}$$

$$^2\mathrm{D} + {}^3\mathrm{T} \rightarrow {}^4\mathrm{He} + \mathrm{n} \quad (17.6\mathrm{MeV}). \tag{1.3}$$

The energy produced in the fusion reaction is carried as kinetic energy of the produced helium nucleus, neutron, and proton.

Deuterium fusion fuel is abundantly available by distillation of all forms of water and, thus, globally available. Tritium is a radioisotope with a 12.5-year half-life and does, therefore, not occur in nature. Tritium can be produced by neutron bombardment of lithium, an abundant element in Earth's crust, in reactor environments. Fusion research typically use deuterium fusion as the conditions resemble reactor-relevant DT fusion but do not require nuclear licensing.

For fusion reactions to occur, the reactant nuclei must be brought within close proximity of one another. By quantum-mechanical tunneling through the repulsive Coulomb potential energy barrier the nuclei become trapped in the potential well of the strong nuclear force and fuse. In *thermonuclear fusion*, the kinetic energy required to fuse the nuclei are provided to the particles as thermal energy in the keV range. Consequently, the fusion fuel exists in the *plasma* state, as a fully ionized gas.

Fusion net power production depends on the plasma density (n) and energy confinement time (τ_E), in addition to requiring plasma tempera-

tures (T) in the keV range. Sufficient plasma temperature and density are necessary to achieve the fusion rates required for power production. In order to maintain fusion-relevant temperatures, the fusion fuel must be heated by the reaction products. The *alpha particle heating*, together with the fusion rate, determines the energy confinement time necessary for net power production via the *fusion triple-product*. The triple-product defines the minimum performance requirements for fusion power production. For DT fusion (Eq. 1.3) the triple-product has a minimum around 14 keV [1]:

$$nT\tau_E \geq 5 \times 10^{21}\ \mathrm{keVsm^{-3}}. \tag{1.4}$$

There are technical and physics challenges associated with achieving $nT\tau_E \geq 5 \times 10^{21}\ \mathrm{keVsm^{-3}}$. The technical challenges include device design, materials, and manufacturing as well as controlling and diagnosing the fusion plasma. The physics challenges include plasma confinement and stability, fuel dilution and contamination, plasma power exhaust, and plasma-wall interaction. Consequently, the highest experimentally achieved fusion triple product is $nT\tau_E \geq 1.5 \times 10^{21}\ \mathrm{keVsm^{-3}}$ [2]. The ITER [3, 4] test reactor, currently under construction in Cadarache, France, is designed to demonstrate the feasibility of fusion power. ITER will provide insight into reactor-relevant plasma physics and yield a ten-fold gain of fusion heating power. This dissertation assesses the physics challenges associated with the reaction chains of hydrogenic molecules that are produced by plasma-wall interaction.

1.1 Magnetic confinement fusion and tokamaks

The leading concept for thermonuclear fusion energy production, adapted by ITER, is *magnetic confinement fusion* using *tokamak* devices. Tokamak devices confine the charged plasma particles in a toroidal magnetic field configuration using external electromagnets (Fig. 1.1); tokamaks are the focus of this dissertation. A central transformer circuit is used to induce a secondary, weaker poloidal magnetic field component perpendicular to the toroidal direction, using the plasma as a secondary circuit. The resulting helical net magnetic field improves the plasma stability and confinement (Fig. 1.1). The helical magnetic field lines, which are nearly aligned with the toroidal direction, create a set of nested toroidal flux-surfaces of constant magnetic flux. Owing to the toroidal symmetry of the plasma, the tokamak geometry can be reduced to a poloidal cross-section by projection of the parallel direction onto the poloidal plane (Fig. 1.2).

Perfect plasma confinement is unattainable due to the turbulent nature of the fusion plasmas. Plasma particles and energy are transported radially outwards in the poloidal plane (Fig. 1.2) due to nonlinear micro-turbulence [5]. Interaction between the plasma and the plasma-facing

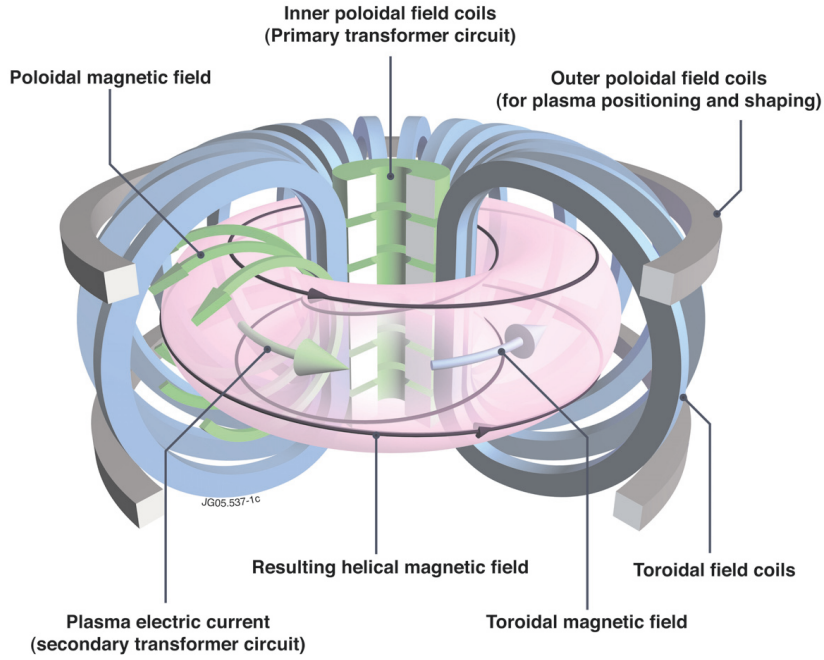

Figure 1.1. Schematic of the magnets and magnetic configuration of a tokamak. ©EUROfusion Consortium.

components (PFCs) sputters wall material, which is detrimental to the performance of the fusion plasma due to fuel dilution and impurity radiation. Therefore, secondary magnets are used to create a figure-eight shape magnetic topology that separates the burning *core plasma* from the PFCs (Fig. 1.2). The flux surface passing through the magnetic null (the *X-point*) is called the *separatrix* and the volume between adjacent flux-surfaces are called *flux tubes* (Fig. 1.2). The *scrape-off layer* (SOL) consists of open flux tubes, radially outside of the separatrix, that diverts the plasma fluxes transported into the SOL to the *divertor targets*, which are PFCs designed to sustain the plasma heat loads (Fig. 1.2). The radial SOL width is typically defined by the radial exponential fall-off length of the plasma heat flux. The SOL width is commonly of the order of millimeters as the plasma velocities parallel to the magnetic field lines are a factor of $\sim 10^4$ larger than the radial velocities. Consequently, the divertor configuration has smaller *plasma-wetted area* compared to the limiter configuration, which increases the plasma heat fluxes to the PFCs. This increase in plasma heat flux is overcome by high target recycling and volumetric momentum and power loss processes in the divertor. The vertical height of the magnetic axis in the poloidal cross-section is defined as the mid-plane (MP) and the volume that is not connected to the core other than through the X-point is called the private-flux region (PFR) (Fig. 1.2).

The toroidal geometry of the tokamak results in magnets spaced more densely closer to the toroidal axis of revolution. Consequently, the magnetic

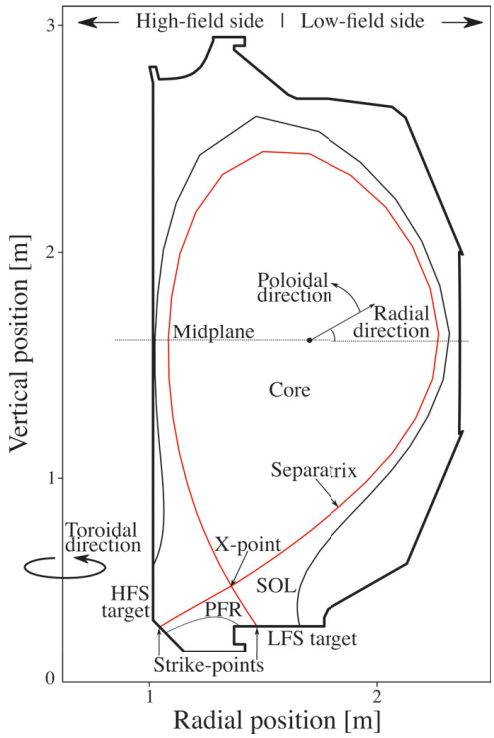

Figure 1.2. Schematic of the poloidal cross-section of the DIII-D tokamak. The labels mark the different regions of the plasma referred to herein.

fields are stronger on the inboard side of the poloidal cross-section, which is typically defined as the high-field side (HFS). Correspondingly, the outboard side of the poloidal cross-section, further from the toroidal axis of revolution, is defined as the low-field side (LFS). Parallel and radial electric fields exist in the SOL due to parallel current densities and gradients in the main ion density and temperature. Together, the non-uniform magnetic field and the electric fields induce transport across the flux-surfaces and, consequently, plasma density, temperature, and radiation asymmetries between the HFS and LFS [6]. When the ion $\mathbf{B} \times \nabla \mathrm{B}$-drift points vertically down towards the lower divertor the cross-field $\mathbf{B} \times \nabla \mathrm{B}$-drifts transports ions across the separatrix into the PFR in the LFS leg. Subsequently, $\mathbf{E} \times \mathbf{B}$ drift flows transport the plasma across the PFR to the HFS divertor leg, yielding higher densities and lower temperatures in the HFS divertor leg compared to the LFS divertor leg [7]. The non-uniform magnetic fields also make the LFS-MP of special interest, due to unfavorable magnetic field curvature relative to the plasma thermal pressure gradient [8]. Consequently, microturbulent radial transport is typically strongest at the LFS-MP, resulting in more core particles and energy entering the SOL at this location, compared to other locations [5]. As the plasma flows from the LFS-MP to the targets, the term *upstream location* is used interchangeably for the LFS-MP.

Plasma transport along the SOL results in a thin (order of 10^{-5} m) region of net positive volume charge in front of the divertor target, called the *electrostatic sheath*. The sheath forms as a result of the large inertia-difference between the plasma ions and electrons, resulting in the electrons reaching the divertor target before the ions, charging it negatively. The negatively charged target attracts the oppositely charged plasma ions, and repels the electrons, resulting in a positive volume charge that shields the upstream SOL plasma from the electric field. Consequently, the sheath accelerates the plasma flow to sonic or supersonic velocities at the sheath entrance, called the Bohm criterion [9, 10, 11]. The plasma potential drop in the sheath and its thickness depend on, among other factors, the electron density, temperature, and ion-electron temperature difference [9].

The volume of the divertor enables volumetric power and momentum exhaust processes along the divertor legs and separates the plasma-surface interaction from the core region. These processes reduce the plasma heat loads to the PFCs, and the separation of the core from the plasma-surface interaction reduces core contamination by radiating impurities. Diverted tokamak plasmas are fueled by plasma recycling at the divertor targets: the plasma ion and electron fluxes impinging on the targets are deposited onto the PFC surfaces, where they readily undergo surface recombination. The resulting neutral particles are emitted into the divertor as molecules and atoms, where they dissociate and ionize, respectively, in the high-temperature plasmas within a short distance of the targets. The ionized particles, constituting a volumetric plasma source, are subsequently accelerated towards the divertor targets by the sheath, creating a recycling loop.

The behavior of the SOL plasma and recycling loop are commonly divided into distinct divertor regimes. These regimes are commonly categorized by their SOL *collisionality* (ν^*_{SOL}), which is a dimensionless quantity describing the number of elastic collisions along the magnetic field lines in the SOL:

$$\nu^*_{SOL} = \frac{L_{SOL}}{\lambda_{mfp}}, \tag{1.5}$$

where λ_{mfp} is the mean-free path of the particles and L_{SOL} the SOL connection length, defined as half the parallel (to the magnetic field lines) distance between the HFS and LFS targets. For fusion applications the ion and electron self-scattering rates (λ_{ii} and λ_{ee}, respectively) are typically taken as the mean-free path, where $\lambda_{ii} \sim \lambda_{ee} \sim 10^{16}\ \mathrm{m^{-2}eV^{-2}T_u^2/n_u}$ and T_u and n_u are the species temperatures and densities at the upstream location.

The plasma flow from the upstream location to the divertor targets is virtually uninhibited, and plasma particle and heat transport is convective, when the collisionality is low ($\nu \lesssim 10$). The heat fluxes incident on the

target are only limited by the sheath and, hence, this regime is called the *sheath-limited regime*. The sheath-limited regime is characterized by an isothermal SOL and a linear dependency of target density on upstream density, $n_t \propto n_u$. At higher SOL collisionality ($\nu > 10$) the plasma heat transport becomes conductive and, thus, limited by the plasma heat conductivity, resulting in parallel temperature gradients along the SOL to sustain the thermal transport. The parallel temperature gradients results in decreased target plasma temperatures and increased target density to conserve the plasma momentum ($n_t \propto n_u^3$), assuming negligible volumetric plasma momentum losses.

The conservation of momentum is, however, only conserved if the SOL is one-dimensional. In the presence of a second, radial direction, as is the case in tokamaks, the net plasma in any give flux-tube is affected by radial transport and viscous friction between adjacent flux-tubes. The decreased target plasma temperature results in increased target plasma flows to maintain the plasma power exhaust through the sheath, assuming negligible volumetric power losses, and increased target recycling. Consequently, this operating regime is called the *high-recycling regime*.

Volumetric plasma momentum and power losses arise at high SOL collisionality ($\nu \gg 10$), reducing both the plasma momentum to the target and the target temperature. The low temperatures at the target are insufficient to ionize the recycled atoms and molecules, resulting in the ionization front moving upstream from the target. The volume between the ionization front and the target in this *detached regime* is dominated by atoms and molecules. The momentum losses, caused by ion-atom and ion-molecule friction, reduces the density at the target and the plasma heat fluxes reaching the PFCs. Combined with the decreased temperature due to radiative power losses, the plasma heat-fluxes reaching the PFCs are reduced to within the divertor target material limitations. This reduction of target heat fluxes makes the detached regime the prospective operational mode of future fusion reactors.

In tokamak experiments the divertor regime is commonly identified by a decrease in electrical Langmuir probe measurements [12] of the target ion saturation flux density (J_{sat}) as a function of increasing upstream density. For attached, i.e. sheath-limited and high-recycling, plasmas the electron temperatures is inferred from the probe measurements but for detached conditions, when the plasma temperature decreases below $\sim$5 eV, the electron temperatures cannot be reliably determined by probe measurements. Hence, plasma characterization is supplemented by electron density and temperature measurements by spectroscopic and Thomson scattering diagnostics, to more accurately determine the plasma conditions. As ion density and temperature measurements typically are not available, the electron temperatures (T_e) and densities (n_e) are commonly taken as representative of the plasma temperature and density, as it is done in

this work unless explicitly stated otherwise. The LFS target is considered the critical indicator of plasmas detachment as the HFS target typically detaches at lower upstream electron density than the LFS target due to cross-field plasma transport caused by $\mathbf{B} \times \nabla \mathrm{B}$-drifts.

1.2 Molecules in fusion plasmas

The hydrogenic molecular species are of special interest in fusion reactors as molecular processes affect the plasma particle, momentum, and power balance. A fraction of the recycled plasma fluxes are returned as molecules, resulting in a molecular source in the SOL. Molecular recycling is strong, up to 90% [13], in devices with carbon-based PFCs, such as DIII–D [14], and molecular processes are expected to be significant. In devices with metallic PFCs, such as JET [15], the molecular recycling is comparably weaker than in carbon-based devices, up to 40% [16, 17, 18]. However, next-step metallic devices, such as ITER and DEMO [19, 20, 21], will operate under detached conditions with target plasma fluxes orders of magnitude larger than that in JET [15]. Thus, molecular processes are expected to be important in both present carbon-lined machines and future metallic devices. This dissertation focuses on understanding and verifying the role of molecular processes in DIII-D to provide insights into the role of molecules in future fusion reactors.

Dissociation of hydrogenic molecules affect the plasma particle balance via multi-step reactions with the plasma electrons and ions involving short-lived "conduit" species, such as H^- and H_2^+. These processes of interest are molecularly-assisted dissociation, recombination, and ionization (MAD, MAR, and MAI, respectively):

$$\mathrm{e}^- + \mathrm{H}^+ + \mathrm{H}_2(v) \rightarrow \ldots \rightarrow 3\mathrm{H} \quad (\mathrm{MAR}), \tag{1.6}$$

$$\rightarrow \ldots \rightarrow \mathrm{e}^- + \mathrm{H}^+ + 2\mathrm{H} \quad (\mathrm{MAD}), \tag{1.7}$$

$$\rightarrow \ldots \rightarrow 2\mathrm{e}^- + 2\mathrm{H}^+ + \mathrm{H} \quad (\mathrm{MAI}). \tag{1.8}$$

Here, $\mathrm{H}_2(v)$ and H represent vibrationally activated, electronic ground state hydrogenic molecules and electronic ground state hydrogenic atoms, respectively. MAR is a volumetric plasma sink and atomic source that occurs at higher plasma temperatures ($\sim$2 eV) compared to electron-ion recombination (EIR, $\sim$1 eV) and, consequently, is of special interest for detachment studies [22, 23, 24, 25]. MAR and MAD compete for the same conduit species and, thus, must be considered simultaneously, whereas MAI is negligible compared to MAD and MAR for typical divertor plasma conditions ($T_e \lesssim 5$ eV, $n_e \gtrsim 10^{20}$ m^{-3}) [26, 27].

Hydrogenic molecules in the SOL also result in plasma energy and mo-

mentum sinks as the molecules are heated and dissociated, respectively. As the plasma ions scatter elastically off the relatively cool recycled molecules, momentum and energy are transferred to the molecules. Plasma energy is also lost as both binding energy to break the covalent inter-molecular bond (dissociation energy $E_{diss} = 4.5\ \mathrm{eV}$) and to kinetic energy of the reaction products upon dissociation. The binding energy is carried as potential energy of the hydrogenic plasma ions and atoms and is released when the ions and atoms recombine into molecules. Under fusion-relevant divertor conditions, recombination into hydrogen molecules is assumed to occur as surface recombination at the PFCs only. Consequently, the binding energy is considered a plasma energy sink. Additionally, the plasma loses power to molecular radiation (Eq. 1.9) and molecularly-induced radiation (Eq. 1.10):

$$\mathrm{e}^- + \mathrm{H}_2(v) \rightarrow \mathrm{e}^- + \mathrm{H}_2^* \rightarrow \mathrm{e}^- + \mathrm{H}_2(v) + \gamma, \tag{1.9}$$

$$\mathrm{X} + \mathrm{H}_2(v) \rightarrow \ldots \rightarrow \mathrm{H}^* + \mathrm{Y} \rightarrow \mathrm{H} + \gamma + \mathrm{Y}, \tag{1.10}$$

where, X represents a plasma electron, ion, or a combination of both and Y the reaction products so that the reaction is balanced, and H_2^* electronically excited hydrogenic molecules. Molecular radiation yields distinguishable molecular emission (e.g., Lyman-Werner and Fulcher series), whereas the molecularly-induced radiation yields atomic emission (e.g., Lyman and Balmer series). Thus, the contribution of molecularly-induced radiation is indistinguishable from atomic excitation-relaxation processes and affect measurements inferred from spectroscopic measurements of the atomic emission.

The molecular structure is more complicated than the atomic structure and consists of electronic levels that are sub-divided into discrete vibrational levels (quantum number v) that has associated discrete rotational levels (quantum number J). The potential of the vibrational levels and the vibrational wave-functions depend on the reduced mass of the molecule and is different for hydrogenic isotopologues (H_2, D_2, T_2, HD, HT, and DT). The potential of the rotational levels depend on the molecular isotopologue, but are equally distributed for all vibrational states. As the energy-difference between rotational levels (order of $10^{-2}\ \mathrm{eV}$) is small compared to the energy-difference between vibrational levels (order of $10^{-1}\ \mathrm{eV}$) the rotational splitting of the vibrational levels are neglected to simplify the subsequent treatment of hydrogenic isotopologues in this work.

The Franck-Condon principle postulates that electronic and vibrational transitions must be compatible with the internuclear configuration of the molecule as these processes are instantaneous compared to the inertial motion of the nuclei [28]. Consequently, electronic and vibrational transitions depend on the overlap integral of the vibrational wave-functions of the initial and final states and, thus, on the hydrogenic isotopologue under consideration. Hydrogen molecular data are the most thoroughly vetted and

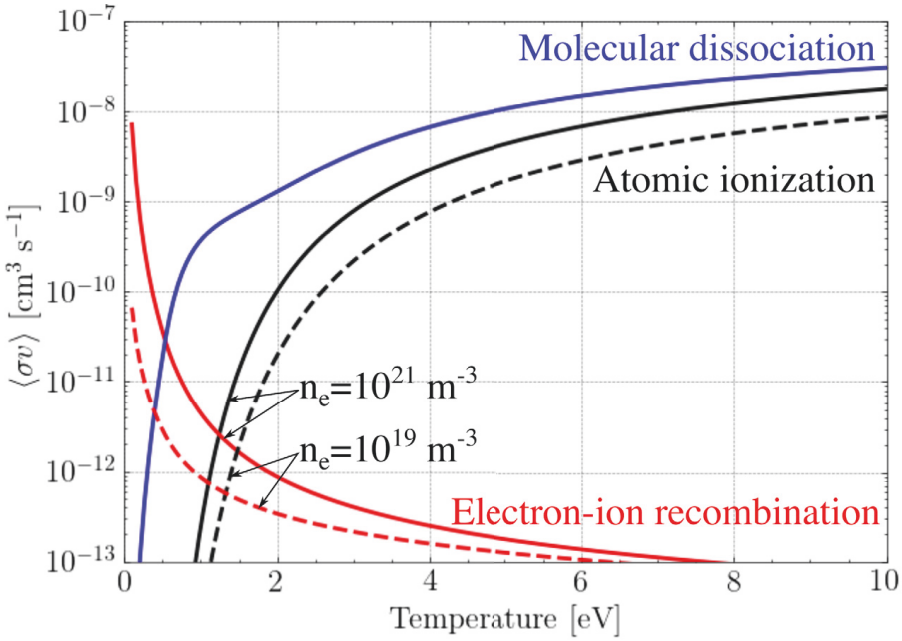

Figure 1.3. Atomic recombination (red), H_2 dissociation (blue), and atomic ionization (black) rates for $n_e = 10^{19}$ m^{-3} (– –) and 10^{21} m^{-3} (–) highlighting the role of molecular processes in the $T_e = 1 - 5$ eV interval. The density-dependence of the dissociation rates is negligible as radiative transitions rates into the molecular ground state are weak.

readily available through a collection of hydrogen rates published in [29]. This comprehensive set of rates, based on experimental measurements of hydrogen, are widely applied within the fusion community. Therefore, the hydrogenic molecular reactions and rates investigated in this dissertation are limited to homonuclear hydrogen molecules (H_2).

Molecular effects are expected to relevant in the temperature range $1\ \text{eV} \lesssim \text{T}_\text{e} \lesssim 5\ \text{eV}$ when EIR and atomic ionization is weak compared to molecular dissociation (Fig. 1.3). In this *molecular-relevant* divertor regime, molecularly-induced volumetric plasma particle, momentum, and power sinks affect the local plasma conditions. At the low-temperature limit ($T_e \lesssim 1$ eV), in the *recombination-dominated regime*, the molecular densities are small compared to the atomic densities as the EIR volumetric atom source is strong (Fig. 1.3). At the high-temperature limit ($T_e \gtrsim 5$ eV), in the *ionization-dominated regime*, the difference between the molecular dissociation and atomic ionization rates are small. Consequently, the molecules and atoms are strongly dissociated and ionized, respectively, resulting in negligible molecular and atomic densities in the plasma (Fig. 1.3). Thus, molecular processes play a negligible role in the recombination and ionization-dominated regimes and are only expected to affect the plasma conditions in the molecular-relevant regime, on which this work focuses.

1.3 Simulating molecules in the SOL of fusion plasmas

Predictive analysis supported by experimental measurements are important tools to assess our understanding and modeling capability of fundamental physical processes in fusion plasmas. As the plasma conditions in next-step tokamaks, such as ITER and DEMO, are unprecedented in existing devices, predictive numerical modeling is important for identifying physical processes that affect the power loads reaching the PFCs, which must be reduced to within the material limitations of the PFCs. Numerical plasma simulations also provide further understanding of the measurements as they predict plasma parameters that are not directly accessible by existing diagnostics. Code-experiment agreement is evaluated using synthetic diagnostics which are compared to actual measurements, providing an indication of our understanding of the physics phenomenon pertaining to the plasma conditions. However, the computational costs of numerical modeling increases with the number of considered processes, physics phenomenon, and device size. Hence, reducing the computational costs of the simulations, while maintaining the predictive capabilities of the codes, is necessary to predict and design future fusion reactions and a topic of this dissertation.

The molecular self-collisionality $\nu^*_{H_2}$, i.e. the self-scattering analogue to the SOL collisionality, is a useful parameter when considering molecular simulations:

$$\nu^*_{H_2} = \frac{L}{\lambda^{H_2-H_2}_{mfp}}. \tag{1.11}$$

Here, L is the characteristic size of the system and $\lambda^{H_2-H_2}_{mfp}$ the molecular self-scattering mean-free path:

$$\lambda^{H_2-H_2}_{mfp} = \frac{v^{H_2}_{th}}{\nu^{H_2-H_2}_{el}} = \frac{\sqrt{2T_{H_2}/m_{H_2}}}{K^{H_2-H_2}n_{H_2}}, \tag{1.12}$$

where $v^{H_2}_{th}$ is the molecular thermal velocity, $\nu^{H_2-H_2}_{el}$ the molecular self-scattering rate, and $K^{H_2-H_2}_{el}$ $[\mathrm{m^3 s^{-1}}]$ the elastic self-scattering coefficient of the molecules.

To assess the full, kinetic time-evolution of the molecules the linearized Boltzmann-like kinetic equation in three spatial and three velocity dimensions needs to be solved for each particle on a static background plasma. This treatment is, however, unfeasible to apply to each individual molecule. Instead, the particles are treated statistically by simulating the individual trajectories of a number test particle histories, each weighted to represent a large number physical particles. The time evolution of the relevant molecular parameters, such as particle and energy density, is subsequently solved from the statistical treatment of the individual test-particle trajectories.

Kinetic models are well-suited for determining the time-evolution of the molecules for low-collisionality (sheath-limited and high-recycling) conditions, as the molecular processes are linear. The computational time of kinetic simulations depend linearly on the molecular-plasma interaction frequency, as every interaction is sampled. However, under conditions of high molecular self-collisionality ($\nu^*_{H_2} \gg 1$), such as detached conditions, the molecular processes become non-linear. Consequently, the computational times of kinetic simulations increase exponentially with the molecular self-collisionality.

Under conditions of sufficiently high molecular self-collisionality ($\nu^*_{H_2} \gg 10$) the molecules are considered Maxwellian and molecular transport is treated by a diffusive fluid approximation [9]. Under this assumption the molecular time evolution of particles, momentum, and energy are solved from the moments of the Focker-Planck kinetic equation [9]. The resulting set of non-linear fluid equations are well suited for describing the behavior of strongly non-linear systems, such as highly collisional molecular populations under detached conditions [9]. Under sheath-limited and high-recycling conditions, however, the molecular collisionality becomes insufficient to warrant a fluid approximation of molecules. Under such conditions a kinetic treatment of the molecular time-evolution is expected to be necessary.

Development of hybrid kinetic-fluid models will decrease the computational cost of numerical simulations while preserving the accuracy of the predictions by utilizing the strengths of both the fluid and kinetic models. These hybrid models may utilize a spatial domain decomposition [30, 31] or a micro-macro decomposition of the kinetic equations [32, 33]. The computational time and accuracy of these hybrid models depend on the accuracy of the fluid model, motivating the development of sophisticated fluid molecular models.

1.4 Scope of the dissertation

This dissertation assesses the role of molecular processes in the SOL of fusion-relevant tokamak plasmas by answering four research questions addressed in five peer-reviewed publications (Tab. 1.1). The role of molecularly induced plasma particle and power sinks and sources are assessed using a fluid molecular model implemented in the multi-fluid edge-plasma code UEDGE [34] (Publication I and II). The fluid molecular model was implemented in UEDGE as the code is publicly available and includes an advanced neutral atomic model coupled to the fluid plasma equations, which was utilized in the development of the fluid molecular model.

UEDGE fluid molecular simulations are verified against simulations using the kinetic neutral code EIRENE [35] to assess the role of kinetic

Table 1.1. Research questions posed in this dissertation and the publications relevant to answering them.

	Research question (RQ)	Publication				
		I	II	III	IV	V
RQ1	How does molecularly-induced plasma sinks and sources affect the SOL in UEDGE simulations?	X	X			
RQ2	Under what conditions is the UEDGE fluid model of molecules applicable?	X	X			
RQ3	Which processes affect the effective molecular dissociation rate?			X	X	
RQ4	What are the effects of including fluid molecules on UEDGE predictions of DIII–D L-mode plasmas?	X				X

transport effects and the applicability of a fluid treatment of molecules in divertor-relevant conditions (Publication I). The role of collisional-radiative processes and assumptions, applied in the kinetic and fluid treatment of molecules, are evaluated by collisional-radiative simulations and kinetic EIRENE simulations (Publication III and IV). The role of molecular processes on the divertor plasma temperature, density, and ion saturation flux is assessed by comparing UEDGE prediction to Langmuir probe and Thomson scattering measurements in DIII-D L-mode plasmas (Publication I and V).

The dissertation provides an overview of the theoretical foundations (Ch. 2) and presents the methods utilized (Ch. 3). The central findings answering the proposed research questions are presented (Ch. 4), their implications discussed, and summarized (Ch. 5). Each subsection of Chapter 4 corresponds to the research question with the corresponding number in Table 1.1.

2. Theory

2.1 Collisional-radiative models for hydrogenic molecules

Fusion-relevant divertor plasmas are too low in temperature and high in density for the atomic and molecular populations to achieve coronal equilibrium, and too hot and tenuous to achieve local thermodynamic equilibrium. Consequently, the atomic and molecular populations in divertor plasmas must be treated by collisional-radiative models [36, 37]. An overview of collisional-radiative modeling for hydrogenic molecules is given here and more complete treatments are found in [38, 39, 40, 41, 42, 43, 44]. The excited molecular states are populated in the CR regime but do not achieve the Maxwell-Boltzmann equilibrium distribution as collisional and radiative processes are in mutual competition. Consequently, ladder-like multi-step processes occur under CR conditions, and knowledge of the collisional and radiative processes is necessary to solve the time-evolution of the atomic and molecular populations:

$$\frac{\mathrm{d}n_k}{\mathrm{d}t} = \sum_{j,l} \mathcal{R}^k_{j,l}(T_j, \dots) n_j n_l + \sum_l A^k_l - n_k \sum_{j,l} \mathcal{R}^l_{j,k}(T_j, \dots) - n_k \sum_l A^l_k + \Gamma_k. \tag{2.1}$$

Here, j represents plasma ions or electrons (i and e, respectively), l is a CR modeled species, $\mathcal{R}^k_{j,l}$ the temperature-dependent reaction rate of reactions involving species and j and l producing species k, and T_j is the temperature of species j. The Einstein coefficient for radiative transitions from species j to k is denoted by A^k_j and Γ_k is an external sink or source of species k. The set of coupled ordinary differential equations (ODEs) in Eq. 2.1 is linearized by assuming the background plasma density and temperature to be time-independent:

$$\dot{\mathbf{n}} = \mathbf{M}(n_e, n_i, T_e, T_i, \dots)\mathbf{n} + \mathbf{\Gamma}(n_e, n_i, T_e, T_i, \dots). \tag{2.2}$$

Here, $\mathbf{n}$ is a vector of the states being modeled, $\mathbf{M}(n_e, n_i, T_e, T_i)$ is the

rate matrix, and $\mathbf{\Gamma}(n_e, n_i, T_e, T_i)$ is a source vector. The rate matrix is constructed based on the rates of the individual collisional and radiative processes and the densities of the plasma background. Therefore, the rate matrix depends on the electron and ion densities and temperatures. The source vector is used to include recombination of the background plasma species into CR modeled species, imposed volumetric sinks or sources, and transport sinks or sources in the system. For completeness all molecular molecular states, including rotationally, vibrationally, and electronically excited molecules, are considered by the CR model. To reduce the complexity of constructing and evaluating the CR system within computational limitation and simplify the discussion, this work simplifies the structure of the hydrogen molecules by neglecting the rotational splitting of the vibrational levels.

CR models are inherently zero-dimensional models and do not evaluate transport of the atomic and molecular species, providing a solution for the system assuming quasi steady-state (QSS) conditions. By coupling the models to transport codes, the effects of transport sinks and sources are included in the $\mathbf{\Gamma}$-term. The time-evolution of the CR system depends on the transport sinks and sources for each of the modeled species, which typically are in excess of hundreds of species. Evaluating the transport of all species is computationally infeasible for existing neutral transport codes, necessitating a reduction in the number of species evolved temporally by the CR model.

Greenland formulated a CR model that separates the species into two subsets: one that must be considered time-dependently (the P-species) and another that are not modeled time-dependently (the Q-species) [38, 39]. The effects of reaction chains involving the Q-species on the P-species time-evolution are considered implicitly by an effective rate matrix ([38], Eq. 2.6–2.9). The validity criterion of the Greenland formulation is given by Eq. 3.25 in [38], for which short life-times are necessary, but not sufficient, for classification as a Q-species. The validity criterion defines the optimal choice of P and Q-species for a valid approximation of the system, ensuring the densities of the Q-species are small compared to the P-species. As the reaction rates are dependent on the plasma parameters, such as temperature and energy, so are the effective rate matrix, the validity criteria, and choice of P and Q-species. The subset of time-dependent P-species is typically relatively small (tens of species) compared to the Q-species (hundreds of species), making the Greenland CR formulation well-suited for coupling to neutral transport codes.

Reactions between two species that do not belong to the plasma background are non-linear and are, therefore, not considered in the linearized set of ODEs (Eq. 2.2). As the background plasma is fixed in the linearization of the ODEs the effect of CR processes on the background plasma density and temperature are assumed to be negligible. The CR treatment

applied throughout this work assumes the volumetric recombination into H_2 to be negligible owing to sufficiently high divertor plasma temperatures and low densities. Presently, reactions involving H_3 are omitted, as H_3 is produced by collisions between the CR-modeled species H_2 and H_2^+ [45]. Non-linear process between CR-modeled species necessitate a time-dependent solution of equation 2.1 or linearization of the equation with respect to either H_2 or H_2^+, in addition to the plasma background species, and is beyond the scope of this work.

2.2 The kinetic neutral transport code EIRENE

This work uses the Monte Carlo neutral code EIRENE to simulate kinetic neutral transport [35]. EIRENE solves a set of coupled Boltzmann-like equations generalized from its original single species form for an arbitrary number of species. The equations consider a bi-linear collision kernel for elastic collisions, corresponding to the Wang-Chang-Uhlenbeck generalization [46, 47], and are linearized by assuming constant plasma ion and electron densities and temperatures. The Wang-Chang-Uhlenbeck generalization includes inelastic and chemical reactions in the multi-species collision kernel, that describe atomic and molecular reactions with the background plasma.

The EIRENE collision kernel is decomposed into sub-kernels based on physical nature of the collision type, such as surface reflection, scattering, atomic, or molecular reactions. When a collision occurs, EIRENE samples the process from the sub-kernels and then samples the post-collision state, i.e. velocity, weight, and species. The reflection kernel is decomposed into a fast reflection, thermal re-emission, and absorption kernel. The reflection sub-kernels are user-defined or based on reflection database, such as TRIM [35, 48, 49]. The atomic and molecular sub-kernels are constructed based on the set of reactions and rates provided to EIRENE by the user.

EIRENE simulates a number (order of 10^5) of test particle histories, each weighted to represent a large number (order of $10^{13} - 10^{16}$) of physical particles, through arbitrary three-dimensional geometries. The test particles are launched from different strata, which represent plasma-facing components, gas puffs, and volumetric or imposed neutral sources. Each test particle trajectory is sampled from an angular and energy distribution and followed on a computational grid with a static background plasma that is supplied to the code. EIRENE samples the trajectory to the collision, which may occur with a surface, the background plasma, or another neutral particle if neutral-neutral (atom-atom, atom-molecule, and molecule-molecules) interactions are considered. At this instance EIRENE calls a neutral-surface, neutral-plasma, or neutral-neutral interaction model, respectively,

and modifies the test particle trajectory and weight accordingly. The test particle histories are tracked until they are absorbed by a surface or react to become a background particle, resulting in a plasma source. The Monte Carlo estimators, describing the number of particles, total momentum, and total energy of the grid cells, are then updated. The neutral properties of interest, such as density, momentum, and temperature are calculated by post-processing of each grid cell.

EIRENE solves the linearized Boltzmann-like equations, necessitating several passes between the plasma and the neutral kinetic codes. This iterative scheme considers the effect of the plasma state on the neutral sinks and sources, and vice versa. The plasma and neutral code are iterated until convergence is achieved, taken to occur when the neutral and plasma sources remain unchanged between iterations. The iterative scheme makes assessing the convergence of the simulations challenging, especially under detached conditions when non-linear effects are significant. If non-linear processes, such as neutral-neutral interactions by the BGK approximation, are considered by EIRENE the non-linear nature of such processes necessitates several internal EIRENE iterations to achieve converged neutral densities.

2.3 The fluid molecular model in UEDGE

Fluid models are well-suited for simulating collisional processes, such as detached divertor plasmas, and achieve numerical convergence rapidly as nonlinear solvers are used. The fluid treatment applies a number of simplifications, such as assuming sufficiently strong self-collisionality of the modeled species for the species to conform to a Maxwellian distribution, to the fundamental Boltzmann transport equation. Therefore, fluid models are limited in their first-principle predictive capabilities and adjustable parameters are used to describe the physical processes affected by the simplifications and assumptions applied: e.g., anomalous radial transport coefficients are used to describe turbulent radial plasma transport. Consequently, fluid models must be used in conjunction with experimental measurements or comprehensive first principle models to validate the choice of adjustable parameters for the parameter space where the fluid model is applied.

This dissertation evaluates the role of molecules in divertor plasmas using the fluid molecular model implemented in the multi-fluid plasma-edge code UEDGE [34]. The model, which self-consistently evaluates the molecularly-induced plasma particle and energy sinks considering CR processes, is based on the diffusive fluid model for molecules first presented in [50] and is presented in detail in Publication I, II, and V.

The UEDGE fluid model for molecules solves the density, velocity, and

energy of the molecules for each cell from Equations 2.3–2.5. The metric coefficients have been suppressed for brevity of presentation and subsonic molecular velocities are assumed.

$$\frac{\partial}{\partial t} n_{H_2} + \nabla \cdot (n_{H_2} \mathbf{v}_{H_2}) = -n_{H_2} \nu_{diss}, \tag{2.3}$$

$$\mathbf{v}_{H_2} = -\frac{\nabla P_{H_2}}{m_{H_2} n_{H_2} \left(\nu_{el}^{H_2-i} + \nu_{el}^{H_2-H} \right)}. \tag{2.4}$$

$$\begin{aligned} \frac{\partial}{\partial t} \left(\frac{3}{2} n_{H_2} T_{H_2} \right) + \nabla \cdot \left(\frac{5}{2} m_{H_2} n_{H_2} \mathbf{v}_{H_2} T_{H_2} - \kappa_{H_2} \nabla T_{H_2} \right) = \\ -\frac{3}{2} n_{H_2} \nu_{eqp} \left(T_{H_2} - T_i \right) - \frac{3}{2} n_{H_2} \nu_{diss} T_{H_2}. \end{aligned} \tag{2.5}$$

Here, $\nu_{diss} = n_e \langle \sigma v \rangle_{diss}(T_e)$ is the dissociation rate, where $\langle \sigma v \rangle_{diss}(T_e)$ is the dissociation rate coefficient and $\nu_{el}^{j-k} = n_k K_{el}^{j-k}$ the elastic scattering rate, and K_{el}^{j-k} is the elastic scattering coefficients between species j and k. P_m is the static molecular pressure and $\nu_{eqp} = K_{el}^{H_2-H} n_a + K_{el}^{H_2-i} n_i$ the equipartition rate, for which the UEDGE assumption of strong ion-atom charge-exchange interactions and thermal equilibration ($T_H = T_i$) is applied. The subscripts H_2, H, i and e refer to the molecules, atoms, ions and electrons, respectively; $\mathbf{v}$ is velocity, and m mass. In equation 2.5, $\kappa_{H_2} = n_{H_2} \chi_{H_2}$ is the thermal conductivity of the molecules, where $\chi_{H_2} = T_{H_2} / \sum_{k \in \{i,H,H_2\}} m_{H_2} \nu_{el}^{H_2-k}$. The model presented in this dissertation considers constant elastic scattering coefficients, $K_{el}^{H_2-k} = 5 \times 10^{-16}\ \mathrm{m^3 s^{-1}},\ k \in \{i, H, H_2\}$.

The molecular momentum is not yet coupled to the ion and atom momentum equations in the UEDGE fluid model. Thus, these coupling terms are omitted from equation 2.4 and the molecular transport is, consequently, purely diffusive. The UEDGE fluid molecular model omits the electronic, vibrational, and rotational splitting of the molecules, evaluating transport ground-state molecules only. To prevent excessive particle, momentum, and energy transport under conditions of low collisionality, the molecular fluxes are limited to the free-streaming fluxes. The transport coefficients are scaled by the factor $(1+|q/q_{fs}|^2)^{-1/2}$, where q is the flux and $q_{fs} = n_k v_{k,th} Q_k$ the corresponding free-streaming flux, $v_{k,th} = \sqrt{T_k e / 2 m_k}$, and Q_k the limited quantity. To provide self-consistent plasma solutions, the UEDGE ion continuity, atom continuity, ion energy, and electron energy equations are balanced by adding the corresponding molecularly-induced sink and source terms to the corresponding equations.

3. Methods

3.1 EIRENE molecular reaction databases and models

EIRENE considers the atomic and molecular reactions defined in the simulation setup. These reactions are user-defined or taken from one of the EIRENE databases HYDHEL [51], H2VIBR [52], and AMJUEL [53]. The HYDHEL database is a digitization of [29] and H2VIBR contains a collection vibrationally resolved molecular data, obtained by re-scaling the rates given for the molecular ground state in [29] by the potential energy of the vibrational state according to [39]. AMJUEL consists of effective atomic and molecular rates calculated using the Sawada CR model [41], considering additional CR reactions such as electronic or vibrational transitions compared to HYDHEL.

The reactions in the EIRENE databases are divided into types depending on the rate or process under consideration. The H.2 reaction rates ($\langle \sigma v \rangle$) are given as a function of the plasma reactant (electron or hydrogen ion) temperature and derived from the corresponding H.1 reaction cross-sections (σ), assuming the individual neutral particles to be at rest ($E = 0.1$ eV) and the plasma reactant distribution to be Maxwellian. Proton-impact reactions given as H.3 reaction rates are a function of both the hydrogen ion temperature and the neutral particle energy. The effective H.4 reaction rates include electronic transitions and assumes the neutral particle to be at rest. Thus, the H.4 reaction rates depend on both electron temperature and density. The H.4 rates do not consider radiative decay back into the molecular ground state, which provides an additional dissociation channel, effectively increasing the dissociation rate. The AMJUEL H.2 and H.4 effective reaction rates may also consider the full vibrational transition matrix, considering transitions between all 15 vibrational states of the H_2 molecule ($v \rightarrow v \pm N,\ N \geq 1$). CR models, such as YACORA [54, 55], can consider the aforementioned processes, including vibrational transitions via electronically excited states. By comparing the effective rates compared

Table 3.1. Reactions considered by the EIRENE Kotov-2008 model. The H_2 depletion reactions are marked with †.

ID	Reaction		ID	Reaction	
H.4 2.2.5g†	$e^- + H_2 \rightarrow e^- + 2H$	[53]	H.2 2.2.12	$e^- + H_2^+ \rightarrow e^- + H^+ + H$	[53]
H.2 3.2.3†	$H^+ + H_2 \rightarrow H + H_2^+$	[53]	H.4 2.2.14	$e^- + H_2^+ \rightarrow H + H(n = 2 - 8)$	[53]
H.2 2.2.17†	$e^- + H_2 \rightarrow H + H^-$	[53]	H.2 7.1.1	$e^- + H^- \rightarrow 2e + H$	[51]
H.4 2.2.9†	$e^- + H_2 \rightarrow 2e + H_2^+$	[53]	H.3 7.2.2	$H^+ + H^- \rightarrow H^+ + e^- + H(n = 2)$	[51]
H.4 2.2.10†	$e^- + H_2 \rightarrow e^- + H^+ + H$	[53]	H.2 7.2.3	$H^+ + H^- \rightarrow H^+ + e^- + H(n = 3)$	[51]
H.4 2.2.11	$e^- + H_2^+ \rightarrow 2e + 2H^+$	[53]			

to those in AMJUEL or H2VIBR the role of these additional processes can be assessed, as was done in Publication IV.

Atomic and molecular (A&M) reaction data are provided to EIRENE in the form of one-dimensional or two-dimensional polynomial fits. The fitting of the A&M data by polynomials necessitates a reduction of data dimensionality to one or two dimensions. Consequently, the fits in the EIRENE databases are truncated by assuming ion-electron equilibration ($T_e = T_i$) and an effective plasma charge of unity ($n_e = n_i$). The electron temperature and density represent the common ion-electron temperatures and densities, unless explicitly stated otherwise. Consequently, molecular reaction rates involving protons consider either electronic transitions or the energy of the molecules, but not both. A&M data can also be supplied to EIRENE as tabulated data files. The tabulation, which presently is limited to the two parameters electron temperature and density, could be extended to consider higher-dimensional data. Throughout this work, the readily available one-dimensional and two-dimensional polynomial A&M data fits in the EIRENE databases are applied.

The EIRENE atomic and molecular model used by Kotov in [56] is widely applied in plasma-edge simulations [22, 57]. This model is herein referred to as the Kotov-2008 model. The Kotov-2008 model considers molecular reaction chains into H atoms and H^+ ions via the charged test species H_2^+ and H^-, that are assumed to be at QSS (Tab. 3.1). The Kotov-2008 model considers elastic scattering of H_2 and H with the background plasma ions and atomic reactions [22, 56]. It does, however, not include neutral-neutral ($H - H$, $H - H_2$, and $H_2 - H_2$) interactions. As a result, the transport of molecules is independent of the atomic populations and vice versa.

Metastable-unresolved and metastable-resolved models

The Kotov-2008 model is *metastable-unresolved* (in, e.g., ADAS [58, 59] terminology) and evaluates the transport and dissociation of a single H_2 species without considering transport of the vibrationally excited populations of electronic ground-state molecules. The effect of vibrational excitation is considered implicitly in the effective rates of the molecular depletion reactions (Tab. 3.2), which are calculated for QSS conditions by

Table 3.2. Reactions included in the metastable-unresolved and metastable-resolved EIRENE setups, respectively. All reaction rate coefficients are taken from [53], except for those marked by †, which are taken from [52]. The reaction prefixes define the reaction type and identifiers in their respective references and v refers to the vibrational state.

Reaction name	Reaction	Metastable-resolved	Metastable-unresolved
Neutral dissociation (ND)	$e^- + H_2 \rightarrow e^- + 2H$	H.4 2.2.5g	H.2 2.vl1†
Ion conversion (IC)	$H^+ + H_2 \rightarrow H + H_2^+$	H.2 3.2.3	H.2 2.vl2†
Dissociative electron attachment (DEA)	$e^- + H_2 \rightarrow H + H^-$	H.2 2.2.17	H.2 2.vl3†
Electron impact ionization (EI)	$e^- + H_2 \rightarrow e^- + H_2^+ + e^-$	H.4 2.2.9	H.2 2.vl4†
Dissociative ionization (DI)	$e^- + H_2 \rightarrow e^- + H + H^+ + e^-$	H.4 2.2.10	H.4 2.2.10

the CR model. At QSS the vibrationally excited, electronic ground-state molecules achieve a CR vibrational equilibrium distribution ($P_{QSS}(v)$) for which the effective rates are calculated as many H_2 reaction rates depend on the vibrational level of the molecules (Ch. 1.3). Transport of metastable states affects the QSS $P_{QSS}(v)$ distribution and, consequently, impacts the effective H_2 rates [60].

The effective reaction rates of the metastable-unresolved H_2 depletion reactions (Tab. 3.2), affecting the vibrational distribution and $P_{QSS}(v)$ are calculated considering different CR processes. The effective reaction rates for neutral dissociation (ND) consider electronic transitions and the full vibrational transition matrix ($v \rightarrow v \pm N,\ N \geq 1$). The effective ion conversion (IC) and dissociative electron attachment (DEA) reaction rates are calculated considering the full vibrational transition matrix without considering electronic transitions. The electron-impact ionization (EI) and dissociative ionization (DI) effective reaction rates are calculated considering electronic transitions assuming the molecules to be in their vibrational ground state.

The metastable-unresolved H_2 depletion reactions assume different vibrational processes and distribution of the electronic ground state H_2. Therefore, the implicit vibrational distribution of this time-dependently evolved molecular species has an effective vibrational distribution different from the local equilibrium vibrational distribution $P_{QSS}(v)$. Consequently, the effective reaction rates predicted by EIRENE are expected to be different from those predicted by CR codes, which assume that the molecules are in local vibrational equilibrium.

The *metastable-resolved* EIRENE model individually considers transport and reaction chains for each of the H_2 vibrational states. To simulate the vibrational states as individual species, vibrationally resolved H_2 depletion rates are necessary and provided by H2VIBR (Tab. 3.2). Vi-

brationally resolved DI rates were not available at the time of writing this dissertation. Hence, the metastable-unresolved DI rates were used for all vibrational states (Tab. 3.2). All other reactions are H.2 type reactions and, thus, not coupled to the electronically excited states. The metastable-resolved model considers ladder-like vibrational transitions ($e^- + H_2(v) \rightarrow e^- + H_2(v' = v \pm 1)$) only. Since all other H_2 reactions are the same for the metastable-resolved and the metastable-unresolved model, differences in the effective molecularly-assisted rates for QSS are attributed to differences in the production of H_2^+ and H^-. If the simulations include transport of metastable states, any differences in the effective dissociation rates predicted by EIRENE are a combination of different H_2^+ and H^- production rates and non-local transport effects.

3.2 The Python collisional-radiative tool CRUMPET

CRUMPET (Collisional-Radiative UEDGE Model for Plasma Edge Theory, Publication I) [61], is a Python tool for creating CR models based on user-defined input. The tool is interfaced with the EIRENE databases and is supplied with user-defined reaction rates and A&M data, from which CRUMPET constructs the CR rate matrix and the external source vector (Eq. 2.2). CRUMPET solves the full CR system assuming QSS, but can apply the Greenland formulation to solve the time-evolution of a user-defined set of P species and can consider externally supplied transport sinks and sources.

Throughout this dissertation, CRUMPET is used to calculate effective H_2 reaction rates for the UEDGE molecular model using the Greenland CR formulation. The UEDGE molecular model assumes the electronic ground state atoms and vibrational and electronic ground state molecules to be the only P species. CRUMPET calculates the molecularly-induced atomic and plasma ion particle sink and source terms from the supplied reactions, including MAR and MAD processes.

CRUMPET self-consistently calculates the molecularly-induced CR energy sink and source terms for the electrons, ions, and atoms, accounting for binding energy and radiative losses. The binding energy is considered a plasma energy sink as the potential energy is released as thermal energy to the PFCs as the ions and atoms undergo surface recombination into H_2 at the PFCs. The molecularly-induced radiation is further decomposed into atomic and molecular lines. The calculation of these energy sinks and sources from a set of coupled ODEs for each energy term is detailed in Publication I, and considers the potential energy of the involved species with user-defined kinetic energy transfer to the reaction products. Here, CRUMPET conforms to the UEDGE assumption of a common temperature for ions and atoms. The energy rate coefficients are calculated from the

effective energy rate matrix in a manner analogous to that presented for the electrons in [39]. Here, the electron energy rates are calculated assuming energy conservation within the system. These effective H_2 energy rates, which are required for the UEDGE fluid molecular model, are not calculated by other CR models, such as YACORA [54, 55].

The effective reaction rates calculated by CRUMPET consider neither ionization or excitation of electronic ground-state atoms nor electron-ion recombination into atomic hydrogen. These processes are considered by the UEDGE fluid atomic model. Consequently, these atomic sinks and sources were omitted to avoid double-accounting for these particle and energy sinks and sources while retaining comparability and compatibility with simulations performed with earlier versions of the UEDGE code.

3.3 UEDGE simulation setup and molecular models

The role of molecules in divertor plasmas is evaluated using the diffusive fluid model for molecules implemented in the multi-fluid plasma-edge code UEDGE (Sec. 2.3). The UEDGE simulations evaluate steady-state plasma conditions. Steady-state is achieved by time-dependently evolving the plasma state at increasing time step with residuals 10^{-8} below their initial values. The molecular processes and boundary conditions assumed in each of the models used in this dissertation are outlined here.

The atom-only model setup

The atom-only UEDGE model does not include molecules as a separate fluid species but, instead, applies an implicit treatment of molecular dissociation by accounting for an electron energy loss and ion-atom energy gain upon ionization. Here, the electron energy loss is taken as 10 eV and the ion-atom energy gain is 5 eV per produced particle. The electron energy loss includes the dissociation (binding) energy and kinetic energy of the reaction products. All electron losses are assumed to heat the ions and atoms to be produced by the implicit dissociation. Consequently, the atom-only model accounts for neither molecularly-induced binding energy, radiative plasma power losses, nor molecularly-induced plasma particle sinks. The implicit dissociation reactions are expected to have a negligible impact on the plasma conditions, as it is treated as an energy transfer from the electrons to the protons and do not result in radiative and binding energy losses. As the electrons and ions in the SOL typically equilibrate in the divertor plasma, the energy lost by the electrons is expected to be offset by the thermal equipartition term, which depends linearly on the ion-electron temperature difference. The atom-only model assumes all ion fluxes incident on the targets to be recycled as atoms.

The DEID model setup

The UEDGE fluid molecular model in [50] assumes molecular dissociation via neutral dissociation only, (HYDHEL reaction H.2 2.2.5) as it is the dominant one-step dissociation process. Thus, the direct-electron impact dissociation (DEID) model assumes dissociation of molecules into two atoms and is a volumetric atom source. The model assumes the dissociation energy (4.6 eV) to be lost by the electrons but gained as kinetic energy of the atoms analogous to the atom-only model. Thus, the DEID model treats dissociation as an energy transfer process between the electrons and the protons, and neglects radiative and binding energy losses. The DEID model assumes all ion and atom fluxes incident on the targets to be recycled as molecules.

The UEDGE-CRUMPET model setup

The fluid model of molecules implemented in UEDGE was extended to consider CR processes, such as MAR and MAI reactions and molecularly-induced plasma energy sinks, by coupling UEDGE to CRUMPET. The UEDGE-CRUMPET model considers effective particle and energy rates calculated by CRUMPET (Sec. 3.2) considering the full set of reaction pathways (Tab. 3.3). Here, the metastable triplet state $\mathrm{c}^3\Pi_\mathrm{u}$ is assumed to have a lifetime of 10 μs, after which it is excited into the $\mathrm{a}^3\Sigma_\mathrm{g}^+$-state, subsequently decaying into the $\mathrm{b}^3\Sigma_\mathrm{g}^+$-state and being dissociated. The populations of the electronic levels above the first excited state are assumed to be small compared to the electronic ground state population and, thus, have a negligible impact on the effective molecular particle and energy rates. Consequently, reactions involving electronically excited levels above the first are omitted by the UEDGE-CRUMPET model. The effective reaction rates are communicated between CRUMPET and UEDGE using tabulated data files, necessitating a reduction in the dimensionality of the data to two. Therefore, the UEDGE-CRUMPET model assumes ion-electron equilibration ($T_e = T_i$) and an effective plasma charge of unity ($n_e = n_i$) to consider data dependent on electron density and temperature only. The UEDGE-CRUMPET model assumes all ion and atom fluxes incident on the targets to be recycled as molecules.

The UEDGE-EIRENE model

The reactions in the UEDGE-EIRENE model are chosen to best correspond to the EIRENE Kotov-2008 model for comparability between the UEDGE and EIRENE molecular simulations, and are a subset of the UEDGE-CRUMPET reactions (Tab. 3.3). The rates considered by the UEDGE-EIRENE model are, however, H.2-type rates (Tab. 3.3) whereas those considered by the EIRENE Kotov-2008 model are H.4-type rates (Tab. 3.1). Thus, the EIRENE model considers additional molecular depletion processes through the electronic excitation of the molecules and off-

Table 3.3. Reactions included in the UEDGE-CRUMPET and UEDGE-EIRENE models. All reactions listed are considered in the UEDGE-CRUMPET model whereas the UEDGE-EIRENE model only consider those marked with †. Here, n denotes the electronic state of the atoms, and v denotes the vibrational state of the molecules. If no state is specified the species is taken to be in its ground state of the relevant quantum number. The ID column lists reaction type and identifier of the process in the listed reference, where applicable. Here, a lifetime of 10 μs is assumed for the $c^3\Pi_u$ metastable triplet state.

ID	Reaction		ID	Reaction	
H.2 2.2.6	$e^- + H_2 \rightarrow e^- + H + H(n = 2)$	[51]		$e^- + H(n > 1) \rightarrow 2e + H^+$	[62]
H.2 2.2.7	$e^- + H_2 \rightarrow e^- + 2H(n = 2)$	[51]	H.2 2.2.8	$e^- + H_2 \rightarrow e^- + H + H(n = 3)$	[51]
H.2 2.2.10†	$e^- + H_2 \rightarrow e^- + H^+ + H$	[51]	H.2 2.v_ivv_f	$e^- + H_2(v_i) \rightarrow e^- + H_2(v_f = v_i \pm 1)$	[52]
H.2 2.vl1†	$e^- + H_2(v) \rightarrow e^- + 2H$	[52]	H.2 2.vl3	$e^- + H_2(v) \rightarrow H + H^-$	[52]
H.2 2.vl4†	$e^- + H_2(v) \rightarrow 2e + H_2^+$	[52]	H.2 2.vl2†	$H^+ + H_2(v) \rightarrow H + H_2^+$	[52]
H.2 3.2.5	$H^+ + H_2 \rightarrow e^- + H^+ + H_2^+$	[51]	H.2 2.2.4	$e^- + H_2 \rightarrow e^- + H_2(EF^1\Sigma_g^+)$	[51]
H.2 2.2.5	$e^- + H_2 \rightarrow e^- + H_2(a^3\Sigma_g^+)$	[51]		$e^- + H_2(v) \rightarrow e^- + H_2(B^1\Sigma_u^+)$	[39]
	$e^- + H_2(v) \rightarrow e^- + H_2(C^1\Pi_u)$	[39]		$e^- + H_2(v) \rightarrow e^- + H_2(c^3\Pi_u)$	[41]
	$e^- + H_2(EF^1\Sigma_g^+) \rightarrow H_2(B^1\Sigma_u^+)$	[41]		$H_2(a^3\Sigma_g^+) \rightarrow H_2(b^3\Sigma_u^+) \rightarrow 2H$	[41]
	$H_2(c^3\Pi_u) \rightarrow H_2(b^3\Sigma_u^+) \rightarrow 2H$			$H_2(B^1\Sigma_u^+) \rightarrow H_2(v)$	[39]
	$H_2(C^1\Pi_u) \rightarrow H_2(v)$	[39]		$H_2(B^1\Sigma_u^+) \rightarrow H_2(b^3\Sigma_u^+) \rightarrow 2H$	[39]
	$H_2(C^1\Pi_u) \rightarrow H_2(b^3\Sigma_u^+) \rightarrow 2H$	[39]	H.2 2.2.11†	$e^- + H_2^+ \rightarrow 2e + 2H^+$	[51]
H.2 2.2.12†	$e^- + H_2^+ \rightarrow e^- + H^+ + H$	[51]	H.2 2.2.13	$e^- + H_2^+ \rightarrow e^- + H^+ + H(n = 2)$	[51]
H.2 2.2.14†	$e^- + H_2^+ \rightarrow H + H(n = 2 - 8)$	[53]	H.2 3.2.6	$H^+ + H_2^+ \rightarrow 2H^+ + H$	[51]
H.2 7.1.1	$e^- + H^- \rightarrow 2e + H$	[51]	H.2 7.1.2	$e^- + H^- \rightarrow 3e + H^+$	[51]
H.2 7.2.1	$H^+ + H^- \rightarrow H^+ + e^- + H$	[51]	H.2 7.2.2	$H^+ + H^- \rightarrow H^+ + e^- + H(n = 2)$	[51]
H.2 7.2.3	$H^+ + H^- \rightarrow H^+ + e^- + H(n = 3)$	[51]		$H(n > 1) \rightarrow H(n' < n)$	[63]

diagonal vibrational transitions considered by the metastable-unresolved model, which are not considered by the UEDGE-EIRENE model (Sec. 3.1). Consequently, the UEDGE-EIRENE rates are approximately equal to the UEDGE-CRUMPET rates at $T_e \approx 1$ eV and approximately a factor of 2 lower than the UEDGE-CRUMPET rates at $T_e = 5$ eV (Fig. 3.1).

3.4 UEDGE modeling of DIII-D plasmas

This dissertation simulates and analyzes a set of well-characterized, lower-single null DIII-D L-mode plasmas. These plasmas were previously analyzed and simulated, for the assessment of molecular radiation to total radiation, using the coupled plasma-fluid, neutral-kinetic code EDGE2D-EIRENE [64]. This dissertation utilizes these deuterium plasmas, as the measurements existed during the course of the work, with intrinsic carbon impurities stemming from plasma-surface interaction with the ATJ graphite plasma-facing components. The plasmas are heated with 0.9–1.1 MW of ohmic heating power, supplemented with 10-millisecond short neutral beam blips with 100 ms intervals for charge-exchange ion-temperature measurements. The plasma current was 1.1 MA, with toroidal field strength of 2.1 T. The ion ∇B drift was in the direction of the lower divertor [65]. Hence, the resulting cross-field drifts yield density, tem-

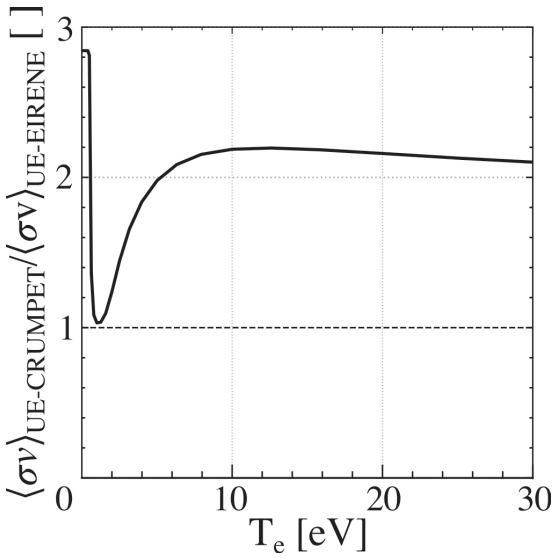

Figure 3.1. Ratio of the UEDGE-CRUMPET effective dissociation rates to the UEDGE-EIRENE effective dissociation rates calculated by CRUMPET as a function of electron temperature. Adapted from Publication I.

perature, and radiation asymmetries between the HFS and LFS divertor legs [66, 67].

To characterize the divertor plasma conditions, the comprehensive suite of lower divertor diagnostics in DIII-D was employed. These diagnostics include the Multi-chord Divertor Spectrometer (MDS) [68], the Divertor Thomson Scattering (DTS) system [69], and target Langmuir probes [12]. The DTS measurements of the LFS target electron temperature (T_e^{LFS-t}) were made approximately 5 mm above the target plate and show T_e^{LFS-t} in a range of 1–30 eV was attained. The LFS-MP electron densities (n_e^{LFS-MP}) were inferred from T_e at the LFS-MP, which was approximated by an extended two-point model relationship [70]. The Langmuir probe measurements of the peak ion saturation current density at the LFS target ($J_{sat,peak}^{LFS-t}$) indicated partial detachment for the highest n_e^{LFS-MP} achieved.

The UEDGE simulations were performed on an EFIT [71] magnetohydrodynamic equilibrium corresponding to DIII-D discharge 160299 at 2230 ms. The simulations consider deuterium plasmas with sputtered carbon impurities. At the core boundary, the constant plasma heating power was 0.9 MW, split evenly between the ions and electrons. The core boundary plasma density was taken as the independent parameter. Upstream density scans were performed by varying the core density to the upper and lower density limits, when convergence could no longer be achieved. The simulations were performed with the cross-field drift terms included to capture the effect of drifts. Radially varying particle and heat diffusivities (in the ranges 0.75–6.6 $\mathrm{m^2 s^{-1}}$ and 1.6–2 $\mathrm{m^2 s^{-1}}$, respectively) were imposed vertically above the X-point. In the divertor, vertically below the X-point,

the particle diffusivity is assumed spatially constant $D_\perp = 1\ \mathrm{m^2 s^{-1}}$. The corresponding heat diffusivities are $\chi_i = 0.75\ \mathrm{m^2 s^{-1}}$ and $\chi_e = 2\ \mathrm{m^2 s^{-1}}$ for ions and electrons, respectively. The global radial viscosity coefficient was taken to be 2.6 $\mathrm{m^2 s^{-1}}$. Albedo-like pumping at the divertor targets provides particle throughput by removing 1% of the assumed Maxwellian atomic fluxes incident on the targets. If molecules are considered as a separate fluid species in the simulations, all atom and ion fluxes impinging on the targets and walls are recycled as molecules in the electronic and vibrational ground state. If molecules are not explicitly included, all ion fluxes recycle as atoms.

4. Results

4.1 Role of molecularly-induced plasma particle and power sinks and sources in UEDGE simulations

Including H_2 molecules as a separate fluid species in UEDGE impacts the plasma solution via the molecularly-induced plasma particle and power sinks and sources. Considering the full set of possible CR reactions in the molecular model is important as the molecularly-induced sink and source terms depend on these reactions. The molecularly induced sinks and sources are under-estimated if only a subset of the molecular reactions is considered compared to if all possible molecular processes are included. Consequently, if only a subset of molecular processes are included in the model, subsequent atomic processes, such as ionization, will be restricted by the dissociation rate, which affects the plasma recycling and particle balance. The role of molecularly-induced plasma sinks and sources is evaluated in a one-dimensional flux-tube using the atom-only and DEID predictions from Publication II, which were repeated using the UEDGE-CRUMPET model. These UEDGE-CRUMPET simulations apply zero radial power-flux conditions at the core boundary, compared to the atom-only and DEID simulations presented in Publication II, which apply zero radial temperature-gradient core boundary conditions. Consequently, the UEDGE-CRUMPET simulations are shifted in the core power-density parameter space compared to the atom-only and DEID simulations and higher core densities are required to attain the corresponding divertor regimes of the simulations presented in Publication II.

Under detached conditions, the DEID model predicts up to one order of magnitude reduction in the target ion density within 50% of the parallel distance between the target and X-point compared to the atom-only model (Fig. 4.1c,f). The decrease in plasma density is caused by an increase in the effective ionization mean-free path as the ionization of the recycled plasma fluxes is limited by the DEID dissociation rate of H_2 . Consequently, the

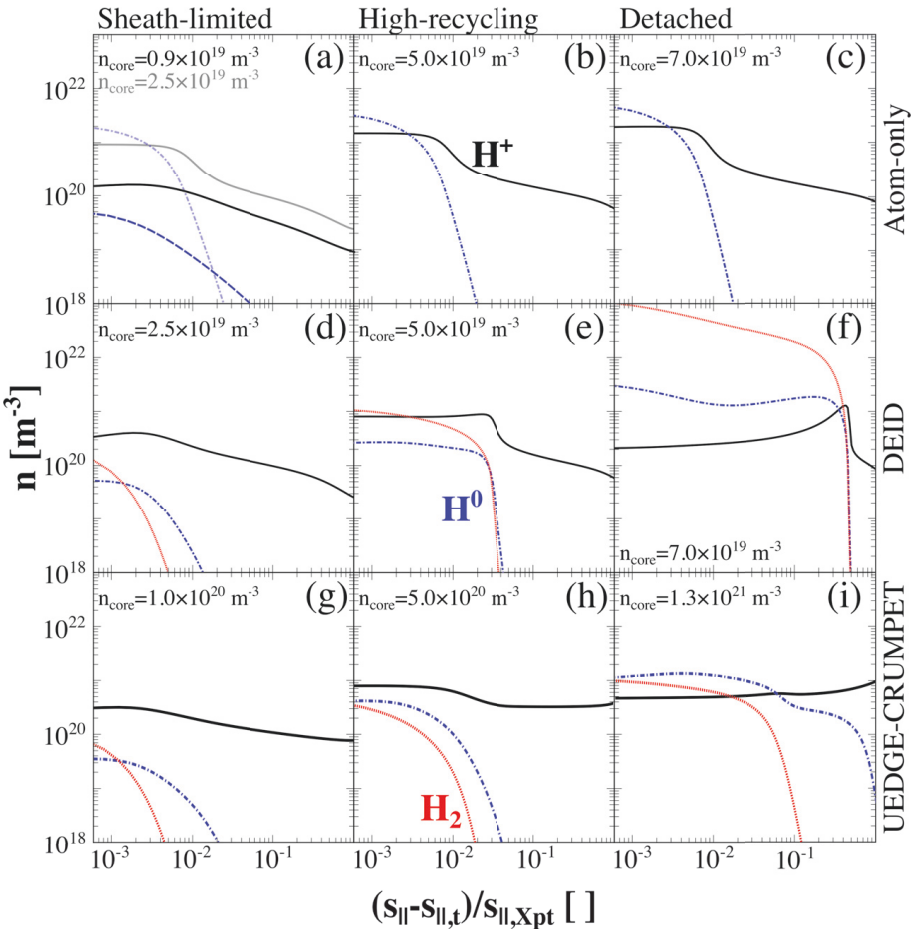

Figure 4.1. Density profiles predicted by UEDGE atom-only (a–c), DEID (d–f), and UEDGE-CRUMPET models (g–i) models as a function of parallel distance from the target normalized to the X-point location ($(s_{\parallel} - s_{\parallel,t})/s_{\parallel,Xpt}$). The ion (black), atom (blue), and molecule (red) profiles are shown on a log-log axis for sheath-limited (a,d,g), high-recycling (b,e,h), and detached (c,f,i) conditions. The original data from Publication II are shown as light blue and grey lines in (a) and is amended with profiles from the simulation with upstream (core) density 9×10^{18} m^{-3}, which correspond to sheath-limited conditions. Adapted from Publication II.

volumetric plasma source due to ionization occurs further upstream in the flux-tube compared to the atom-only predictions, which decreases the target plasma densities and recycling flux. Under sheath-limited conditions the plasma temperatures are sufficiently high to dissociate the molecules and ionize the atoms within 1% of the parallel distance from the target to the X-point, similar to the atom-only predictions (Fig. 4.1a,d). The lower temperatures ($T_e < 5$ eV) under high-recycling conditions results in weak dissociation of the molecules and an increased effective ionization mean-free path of the recycled particles. Consequently, the plasma ionization source is predicted to occur at 4% of the poloidal distance from the target to the X-point for the DEID model compared to 1% for the atom-only model (Fig. 4.1b,e). This strong detachment of the ionization front is qualitatively different than observed in the atom-only model, indicative of the effect being due to molecular dissociation limiting the atom source.

The UEDGE-CRUMPET model predicts distinct detachment as molecular and atomic densities dominate 10% of the parallel distance to the X-point closest to the target (Fig. 4.1i). A similar distinct detachment is observed in the DEID simulations (Fig. 4.1f,i) but not for the atom-only simulations for the simulated upstream (core) density interval (Fig. 4.1c). Under sheath-limited conditions, the UEDGE-CRUMPET simulations are qualitatively similar to the atom-only and DEID simulations. This observation is indicative of the role of molecular processes being small owing to high plasma temperatures (Fig. 4.1a,d,g). Under high-recycling conditions, the CR processes considered by the UEDGE-CRUMPET model increases the dissociation rate (Fig. 4.2), which reduces the H_2 densities by a factor of 3 compared to the DEID model (Fig. 4.1e,h). The increased dissociation rate also reduces the H_2 density below the plasma and atom densities, resulting in closer qualitative agreement of the plasma densities with the atom-only model than the DEID model (Fig. 4.1b,e,h). This finding is indicative of molecular dissociation in the UEDGE-CRUMPET simulations not limiting the plasma ionization, resulting in a negligible increase in the effective ionization mean-free path of the recycled particles, under sheath-limited conditions. Under detached conditions, UEDGE-CRUMPET predicts the molecularly-induced plasma particle and power sinks and sources to reduce the molecular density by up to two orders of magnitude compared to the DEID model (Fig. 4.1f,i).

The DEID model under-estimates the dissociation rate by up to two orders of magnitude in the molecular-relevant regime ($1\ \mathrm{eV} < \mathrm{T_e} < 5\ \mathrm{eV}$) compared to the UEDGE-CRUMPET model (Fig. 4.2a). Consequently, the effective ionization mean-free paths of the recycled particles predicted by the DEID model are longer than those predicted by the CRUMPET-UEDGE model, consistent with the predictions (Fig. 4.1). For temperatures in excess of 15 eV the DEID dissociation rate is under-estimated by several orders of magnitude compared to the UEDGE-CRUMPET rates, as

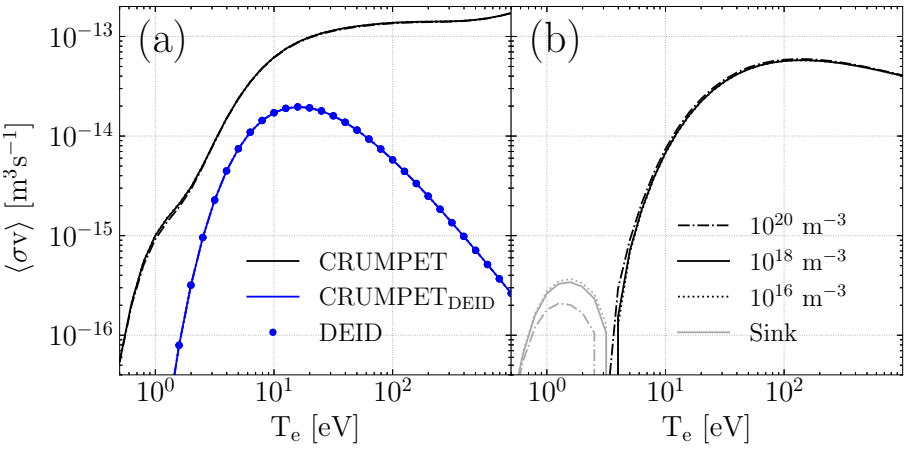

Figure 4.2. Atom (a) and ion (b) particle source rates from dissociated molecules predicted by the UEDGE-CRUMPET (black) and DEID (blue) models for plasma densities 10^{16}, 10^{18}, and 10^{20} m^{-2} taken from Publication I. The grey segments represent negative sources, i.e. sinks.

CR processes dominant at temperatures in excess of 10 eV considered by UEDGE-CRUMPET are neglected by the DEID model (Fig. 4.2a). The UEDGE-CRUMPET model considers MAR rates, which results in dissociation rates a factor of two higher compared to the DEID model at $T_e = 1$ eV. The role of proton-impact reactions, the main MAR channel, is dominant for $1\ \mathrm{eV} \lesssim \mathrm{T_e} \lesssim 3\ \mathrm{eV}$ which is observed as an ion sink term and atom source term (Fig. 4.2a–b). The MAD and MAI ion sources are, however, negligible compared to atom source from molecular dissociation (Fig. 4.2a–b). However, MAD competes for the same reactants as the MAR reaction and even so limits the strength of the MAR reactions, which is reason to consider the full CR system.

The DEID model predicts lower hydrogenic radiative power losses compared to the atom-only model as the atomic densities are limited by the dissociation rate (Figs. 4.3a,b and 4.2a). Consequently, higher upstream (core) densities are necessary to achieve similar hydrogenic power losses in the DEID model as in the atom-only model. The lower dissociation rate results in high molecular densities and strong thermal coupling of the molecules to the plasma ions and atoms compared to the UEDGE-CRUMPET predictions (Fig. 4.1e,f). The thermal equipartition transfers power to the molecules, cooling the ions and atoms, which have a common energy equation in UEDGE (Fig. 4.3b). Consequently, the ion-electron thermal equipartition strength is lower in the DEID model compared to the atom-only model as the thermal energy of the ions is lower (Figs. 4.3b). The thermal losses to the high-density molecular fluid are sufficient to produce detachment-like conditions, although there is no physics basis for this behavior as it stems from an under-estimation of the dissociation rates.

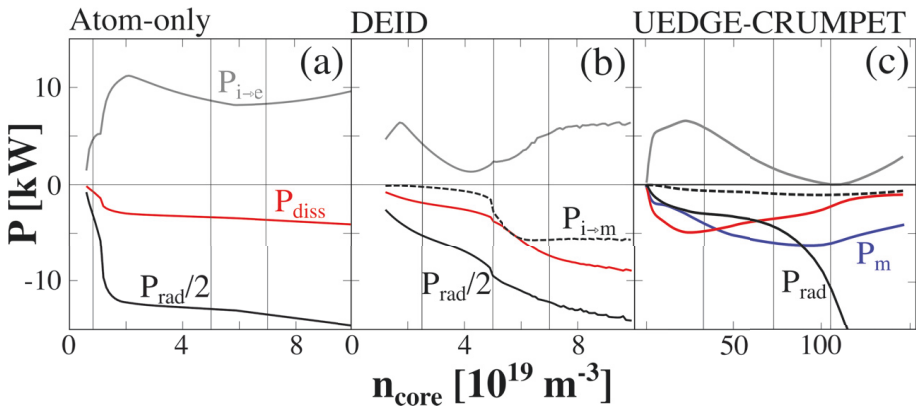

Figure 4.3. Electron power sinks and sources predicted by the atom-only (a), DEID (b), and UEDGE-CRUMPET (c) models as a function of upstream (core) density. Positive values indicate electron power gain through ion-electron thermal equipartition (grey), whereas negative values represent electron power losses due to hydrogen radiation (black) and molecular interactions (red), and ion power losses due to ion-molecule thermal equipartition (dashed line). The molecularly-induced plasma power loss due to molecularly-induced atomic radiation, molecular radiation, and molecular binding potential is also shown (blue). Adapted from Publication II.

The UEDGE-CRUMPET simulations predict the molecularly-induced plasma losses, dominated by binding energy losses (Fig. 4.4c,d), to be comparable to the hydrogenic radiative losses under sheath-limited and high-recycling conditions (Figs. 4.3c). The difference between the electron power losses due to molecular interactions (Figs. 4.3c, red curve) and the molecularly-induced losses (Figs. 4.3c, blue curve) represents an ion power source when the electron power losses due to molecular interactions dominate. Correspondingly, the difference represents an ion power sink when the molecularly-induced losses dominate. The molecularly-induced power losses reduce the plasma temperature, leading to the achievement of the recombination-limited regime, which is characterized by a strong increase in the hydrogenic radiative losses (Figs. 4.3c). Under recombination-limited conditions the strength of molecularly-induced power sinks decreases with increasing upstream (core) density, as the divertor conditions are dominated by atomic processes. The increased molecular dissociation rate considered by the UEDGE-CRUMPET model compared to the DEID model results in negligible ion-molecule thermal equipartition, as the molecular densities are comparably low (Figs. 4.3c). The ion-electron thermal equipartition strength is also decreased, as molecularly-induced power sinks exhaust power that was previously transferred between the ions and electrons (Figs. 4.3c).

Approximately 50% of the molecularly-induced electron power losses are exhausted from the plasma as binding energy losses for $T_e \gtrsim 2$ eV, the other ~50% via heating of the ions and atoms (Fig. 4.4a–c). This binding energy cannot be directly measured using spectroscopy or bolom-

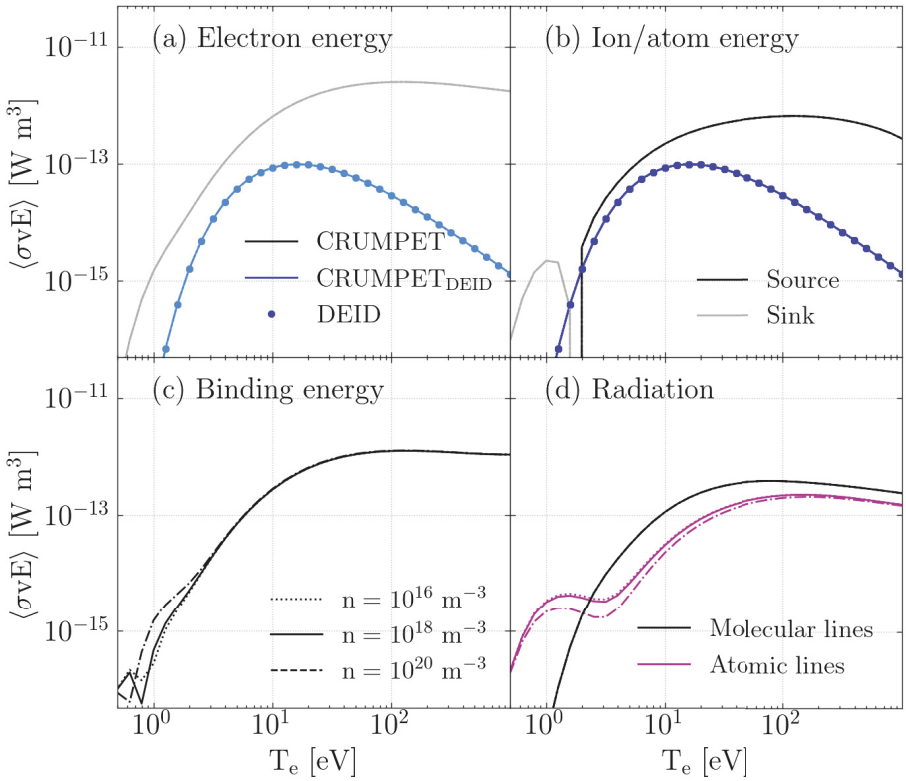

Figure 4.4. Molecularly-induced electron (a), ion-atom (b), binding energy (c), and radiation (d) source rates predicted by the UEDGE-CRUMPET (black) and DEID (blue) models for plasma densities 10^{16}, 10^{18}, and 10^{20} m^{-2} taken from Publication I. The light blue and grey segments represent negative sources, i.e. sinks. Also shown are the atom source for the DEID model from the source data and evaluated using CRUMPET. Taken from Publication I

etry. Therefore, the sum of the measured radiated divertor power and target energy fluxes is expected to be smaller than the power entering the divertor when molecular recycling is strong, as in carbon devices. The radiative losses considered by the UEDGE-CRUMPET model is dominated by H_2 radiation for $T_e \gtrsim 2$ eV, but the radiated energy is negligible compared to the energy lost as binding energy (Fig. 4.4c–d). For $1\ \mathrm{eV} \lesssim \mathrm{T_e} \lesssim 3\ \mathrm{eV}$, proton impact reactions are dominant, resulting in molecularly-induced power losses (Fig. 4.4b) consistent with the observations in Figure 4.3. The molecularly-induced losses are dominated by radiative losses for $T_e \lesssim 2$ eV, which are lost as atomic radiation, stemming from excited atomic reaction products. The molecularly-induced atomic radiation, carrying most of the molecularly-induced plasma energy losses, is spectroscopically indistinguishable from atomic line radiation due to electronic excitation followed by radiative relaxation. Consequently, the spectroscopically inferred atomic and molecular densities are over-estimated and under-estimated, respectively, compared to the experimental atomic and molecular densities if the molecularly-induced radiation is not accounted for. It should be pointed out that the energy rates presented in Figure 4.4 must be scaled by the molecular densities when evaluating the magnitude of the radiative power losses. Thus, the role of the processes discussed are only expected to be significant when the molecular densities are high or, alternatively, when molecular recycling is dominant and $1\ \mathrm{eV} \lesssim \mathrm{T_e} \lesssim 5\ \mathrm{eV}$.

4.2 Verification of the UEDGE-CRUMPET fluid molecular model against EIRENE kinetic neutral simulations

Comparison of the molecular content predicted by UEDGE and EIRENE

The applicability of the fluid molecular model in UEDGE is assessed by verifying the UEDGE predictions against kinetic EIRENE simulations. The simulations were performed for a $0.1\ \mathrm{m} \times 0.1\ \mathrm{m}$ Cartesian domain with a source of ground-state H_2 molecules at the cell center. The boundaries are purely absorbing to assess the effects of dissociation and transport between the models without considering differences in the boundary conditions between EIRENE and UEDGE. The UEDGE simulations were performed using UEDGE-CRUMPET rates and UEDGE-EIRENE rates, which were chosen to best replicate the reactions included in EIRENE, as calculated by CRUMPET (Sec. 3.3). Spatially and temporally constant plasma density and temperature distributions are prescribed and a parameter scan in temperatures is performed for plasma density $n_e = 1 \times 10^{18}\ \mathrm{m}^{-3}$. Further temperature scans for other plasma densities are presented in Publication I.

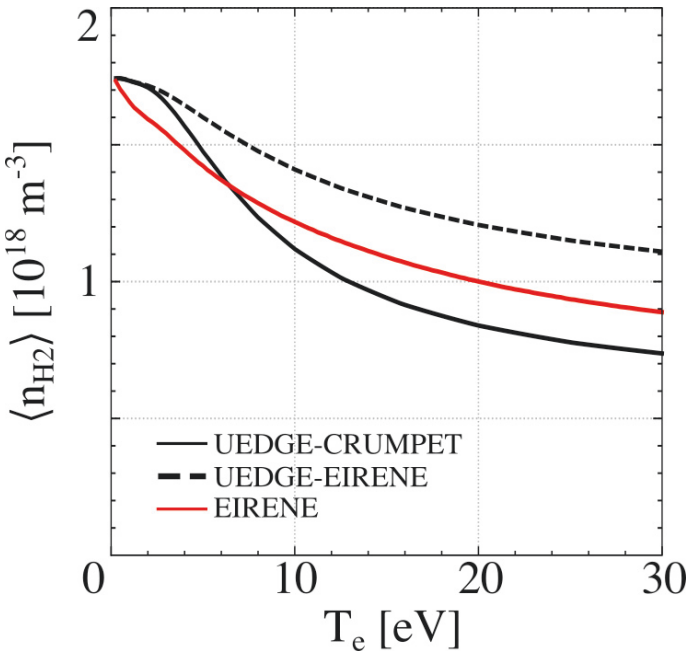

Figure 4.5. Comparison of UEDGE (black) and EIRENE (red) mean H_2 densities for $n_e = 1 \times 10^{18}$ m^{-3} as a function of the electron temperature prescribed in the domain. UEDGE predictions for the UEDGE-CRUMPET (solid) and UEDGE-EIRENE (dashed) predictions are shown. Adapted from Publication I

The time-evolution of the molecular content (N_{H_2}) in terms of the sink and source terms is expressed as:

$$\frac{\mathrm{d}N_{H_2}}{\mathrm{d}t} = S_{source} + S_{diss} + S_{wall} = 0. \tag{4.1}$$

Here, S_{source} describes the central H_2 source, $S_{diss} = n_{H_2} n_e \langle \sigma v \rangle_{diss}(T_e) V$ the net dissociation rate of molecules and V the domain volume, and S_{wall} the particle pumping rate at the wall, which equals the molecular fluxes reaching the wall as all wall fluxes are absorbed. The second equivalence stems from the simulations being performed for steady-state conditions. As the particle source is identical between the codes, the H_2 content is determined by the dissociation and wall transport rates.

The UEDGE-CRUMPET and UEDGE-EIRENE H_2 content predictions are within 10% and 15% of the EIRENE-predicted H_2 content for $T_e < 10$ eV, respectively (Fig. 4.5). The UEDGE-CRUMPET H_2 content predictions are lower than the UEDGE-EIRENE predictions, consistent with the difference in dissociation rate due to higher H_2 depletion rates considered by the UEDGE-CRUMPET model compared to the UEDGE-EIRENE model (Fig. 3.1). The UEDGE-EIRENE predictions for H_2 content are higher than the EIRENE predictions, despite the same reactions being considered by the models. However, the UEDGE-EIRENE rates employ H.2 rates from HYDHEL whereas EIRENE uses AMJUEL H.2 and H.4

rates. The AMJUEL rates consider additional CR processes and dissociation channels compared to the HYDHEL rates, such as vibrational and electronic transitions, resulting in a higher effective dissociation rate for the AMJUEL rates compared to the HYDHEL rates (Ch. 3.1 and 3.3). The UEDGE-CRUMPET predictions for H_2 content is lower compared to the EIRENE predictions for $T \gtrsim 5$ eV, consistent the additional CR processes considered by the UEDGE-CRUMPET model increasing the effective dissociation rate. For $T \lesssim 5$ eV the UEDGE-CRUMPET H_2 content predictions are, however, up to 10% higher than EIRENE prediction despite consideration of additional CR processes by UEDGE-CRUMPET. As $T_e \to 0$ eV, the H_2 dissociation sink becomes negligible ($S_{diss} \to 0$ s^{-1}), resulting in $S_{wall} \gg S_{diss}$ and the H_2 content being determined by wall transport. Therefore, the wall sink in EIRENE is stronger than in the UEDGE-CRUMPET simulations as the EIRENE molecular transport is kinetic whereas the UEDGE molecular transport is assumed diffusive for $T \lesssim 5$ eV (Eq. 4.1).

These results indicate that the effect of the CR processes considered in the dissociation rates used in the fluid UEDGE model is greater than the kinetic transport effects for $T \gtrsim 5$ eV. Kinetic transport effects become dominant for $T \lesssim 5$ eV as S_{diss} depends on the plasma temperature. The temperature for the transport-dissociation transition depends on the plasma density, as S_{diss} has a plasma density dependence. Including neutral-neutral interactions in the EIRENE simulations, which are assumed in the UEDGE fluid model, or changing the molecular elastic scattering rates used by UEDGE could likely reduce the differences in particle transport between the models.

Comparison of the mean molecular energy predicted by UEDGE and EIRENE

Analogous to the molecular density, the net molecular energy ($E_{H_2,tot}$) is determined by:

$$\frac{\mathrm{d}E_{H_2,tot}}{\mathrm{d}t} = P_{source} + P_{i-H_2} + P_{H-H_2} - P_{diss} + P_{wall} = 0. \tag{4.2}$$

Here, $P_{source} = S_{source}E_{source}$ is the source power due to the particle source, $E_{source} = 3T_{source}/2$ the energy of source particles, and P_{i-H_2} and P_{H-H_2} the ion-molecule and atom-molecules thermal equipartition, respectively. The dissociation power sink is $P_{diss} = |S_{diss}|\, E_{H_2}$, where $E_{H_2} = 3T_{H_2}/2$ is the local H_2 energy, and P_{wall} the net energy flux onto the wall. Here, we consider the total thermal equipartition of the molecules $P_{eqp} = P_{i-H_2} + P_{H-H_2}$: as the EIRENE model used does not consider neutral-neutral interaction, $P_{H-H_2} = 0$ for EIRENE. In EIRENE, the source H_2 are assigned $E_{source} = 0.1$ eV, whereas E_{source} in UEDGE is determined by the local molecular energy and is, thus, coupled to the other terms.

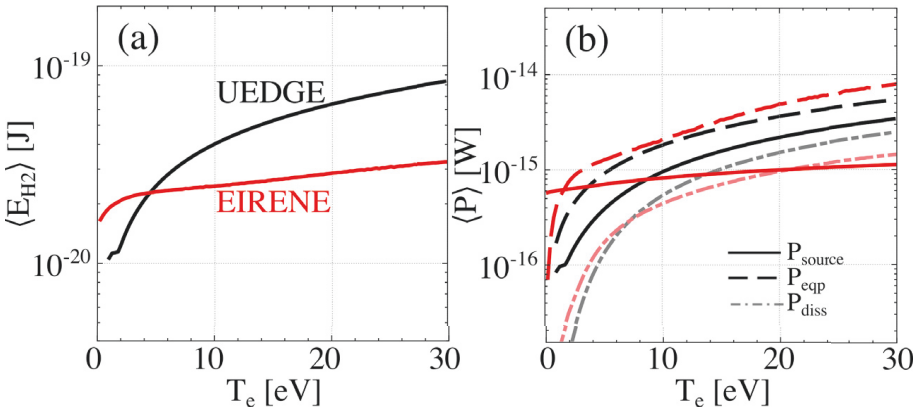

Figure 4.6. Mean H_2 energy content (a), mean H_2 power source ($\langle P_{source} \rangle = P_{source}/N_{H_2}$) from the particle source (–), mean H_2 power source due to thermal equipartition ($\langle P_{eqp} \rangle$, – –), and mean H_2 dissociation power sink ($\langle P_{diss} \rangle$, – · –) predicted by the UEDGE-EIRENE model (black) and EIRENE (red) for $n_e = 1 \times 10^{18}$ m^{-3}. Note the logarithmic abscissae. Negative source terms, i.e. sinks are marked by light red and grey lines. Adapted from Publication I.

The UEDGE-EIRENE and EIRENE predictions of the mean H_2 energy ($\langle E_{H_2} \rangle = E_{H_2,tot}/N_{H_2}$) lie within a factor of 2 for temperatures corresponding to the molecular-relevant regime ($1\ \text{eV} \lesssim T_e \lesssim 5\ \text{eV}$, Fig. 4.6a). Here, the mean H_2 energy predicted by UEDGE-EIRENE is taken as representative of the UEDGE-CRUMPET predictions and presented, as the models predict similar mean molecular energy. Conductive and convective power transport out of the domain are the dominant energy loss channels as the central source is within close proximity of the absorbing domain boundaries. Consequently, the resulting mean molecular energy is low compared to the power sources (Fig. 4.6a,b). The EIRENE and UEDGE predictions for the H_2 thermal equipartition power source, which is the dominant molecular energy source, and the H_2 dissociation power sink are within a factor of 2 for molecular-relevant conditions ($1\ \text{eV} \lesssim T_e \lesssim 5\ \text{eV}$) and $n_e = 1 \times 10^{18}$ m^{-3} (Fig. 4.6b). The mean H_2 energy does not correspond to the sum of the H_2 particle source source, equipartition, and dissociation power sinks and sources (Fig. 4.6b). The discrepancy is due to differences between the wall sources (Eq. 4.1) in UEDGE and EIRENE. EIRENE considers kinetic energy transport effects whereas UEDGE assumes diffusive thermal transport.

The molecular self-collisional mean-free path predicted by UEDGE-EIRENE is $\lambda_{mfp}^{H_2-H_2} \gtrsim 4$ m at $T_e < 5$ eV (Eq. 1.12), for which wall transport is the dominant loss process (Fig. 4.5), resulting in $\nu_{H_2}^* < 1$ (Eq. 1.11). The low $\nu_{H_2}^*$ is attributed to the domain size and the elastic self-scattering coefficient ($\nu_{H_2}^* \propto LK_{el}^{H_2-H_2}$, Eq. 1.11). The small domain size results in close proximity of the molecular source to the absorbing domain boundaries and pumping of the molecules before they can establish a Maxwellian distribution. The UEDGE elastic scattering rate coefficient is assumed

to be constant $K_{el}^{H_2-H_2} = 5 \times 10^{-16}\ \mathrm{m^3 s^{-1}} \ll \langle \sigma v \rangle_{diss}$ (Fig. 4.2). Thus, the molecules are predominant dissociated rather than elastically scattered. Consequently, the molecular energy and velocity distributions will conform to the wall or source distribution rather than establish a Maxwellian distribution. Under conditions of strong ion-molecule and atom-molecule scattering, the molecular velocity and energy distribution will be shifted to the ion and atom distributions.

The molecular content and mean energy predicted by UEDGE are within 15% and a factor of 2 of the EIRENE predictions, respectively, despite molecular self-collisionalities insufficient to establish a Maxwellian distribution, which is the assumed distribution of the molecules in the diffusive fluid model. The EIRENE model used does, however, not consider neutral-neutral ($\mathrm{H-H}$, $\mathrm{H-H_2}$, and $\mathrm{H_2-H_2}$) interactions. Neutral-neutral interactions are an underlying assumption for the UEDGE fluid model and including them in the EIRENE simulations is expected to improve the agreement between EIRENE and UEDGE. In the UEDGE model, energy transport and transfer between molecules and ions depend on the elastic self-scattering rates of $\mathrm{H_2}$ and $\mathrm{H_2}$ elastic scattering with ions, respectively (Eq. 2.5). Considering temperature-dependent molecular elastic scattering rate coefficients from available A&M data in the UEDGE molecular model is expected to increase the molecular self-collisionality and ion-molecule thermal equipartition, consequently improving the agreement between UEDGE and EIRENE. Additionally, a set of fluid equations for non-Maxwellian molecular distributions could be derived and applied under conditions when the molecules are non-collisional.

4.3 Impact of collisional-radiative processes on the effective dissociation rate

Assessing the impact of the processes considered by the CR models and the assumptions made when coupling the CR model to the transport code is important to understand the role of CR models in fusion plasma simulations. The CR codes communicate with the UEDGE and EIRENE transport codes via parametrized fits and data tables which are calculated assuming a $T_e = T_i$ and $n_e = n_i$. The reactions given in the EIRENE A&M databases consider different CR processes, which affect the effective dissociation rates. The effective rates are calculated from CR models assuming QSS conditions, which generally do not hold as metastable states are affected by non-local transport effects.

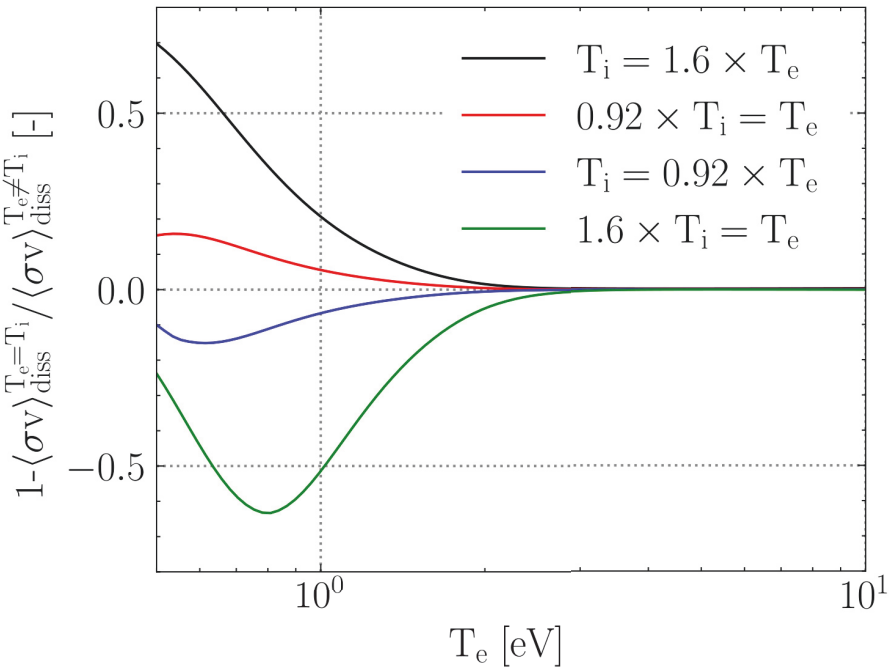

Figure 4.7. Ratio of effective H_2 dissociation rates for equilibrated plasmas to that of unequilibrated plasmas predicted by CRUMPET as a function of electron temperature for $n_e = 1 \times 10^{20}$ m^{-3}. Note the logarithmic ordinate.

Impact of ion-electron thermal equilibration on the effective dissociation rate

CRUMPET calculations, using the UEDGE-CRUMPET model, indicate the degree of ion-electron thermal equilibration (T_i/T_e) to affect the effective dissociation rate when $T_e \lesssim 3$ eV (Fig. 4.7). Proton-impact reactions are relevant for $T_e \lesssim 3$ eV, but negligible for $T_e \gtrsim 3$ eV. Therefore, the effective dissociation rate depends on T_i/T_e for $T_e \lesssim 3$ eV only. In the recombination-dominated regime ($T_e \lesssim 1$ eV), atomic processes are dominant. Consequently, the role of ion-electron thermal equilibration is expected to be relevant in the temperature interval $1\text{ eV} \lesssim T_e \lesssim 3\text{ eV}$, in which CRUMPET predicts a 60% degree of thermal equilibration to affect the effective dissociation rates by a factor of up to 2 (Fig. 4.7).

Plasma temperatures below 3 eV are achieved close to the target for detached divertor conditions only (Fig. 4.8c). Consequently, the effect of ion-electron thermal equilibration on the effective dissociation rates are only expected to be relevant for a fraction of the divertor volume. However, as the plasma is recycled as molecules at the targets, where the plasma temperatures are lowest, the recycled molecules are expected to interact with $T_e \lesssim 3$ eV plasmas. Thus, the effect of ion-electron thermal equilibration may impact the effective dissociation rate under detached conditions. Here, the UEDGE simulations are performed with the atom-

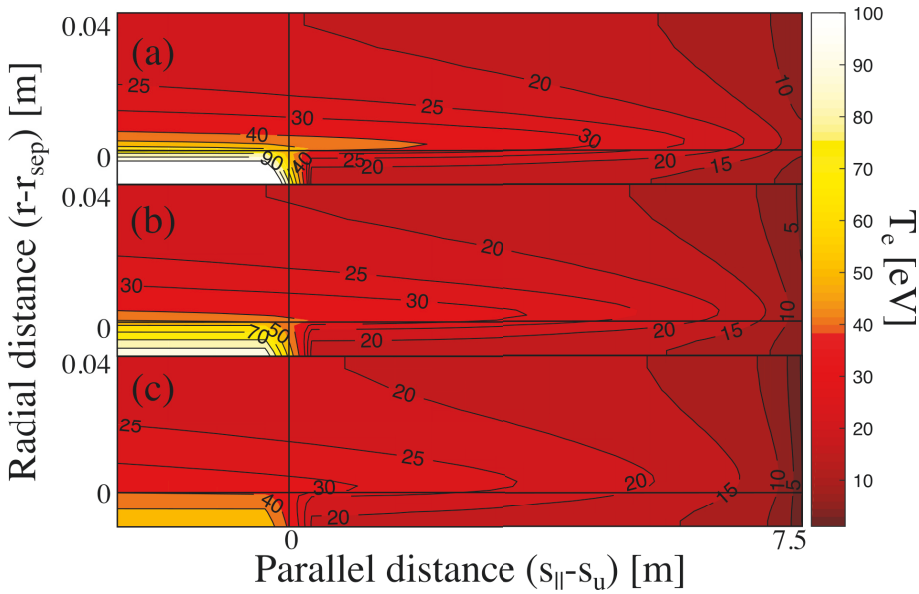

Figure 4.8. Electron temperature surfaces for sheath-limited (a), high-recycling (b), and detached (c) two-dimensional UEDGE simulations using the atom-only model. The X-point is located at $s_{\|} - s_u = 0$ m and the target at $s_{\|} - s_u = 7.5$ m. Adapted from Publication III.

only model, as the simulations were performed before the fluid molecular model was implemented in UEDGE.

UEDGE predicts the $T_i/T_e = 1.6$ in the regions of $T_e < 3$ eV under detached conditions (Fig. 4.9c). The electron inertia is low compared to the ions ($m_i/m_e \approx 2000$), resulting in stronger conductive parallel power transport from the upstream to the target. The stronger parallel power transport results in lower upstream temperatures and smaller temperature gradients along the SOL for the electrons compared to the ions. Therefore, T_i is higher than T_e at the upstream and T_i is lower than T_e at the target in the absence of power losses along the SOL.

UEDGE predicts that the weak parallel power transport results in long parallel energy confinement times of the ions compared to the electrons. Consequently, the ion radial power losses along the SOL are higher than the electron radial power losses close to the separatrix, heating the ions in the far-SOL and PFR (Fig. 4.9). The stronger radial ion power transport compared to the electrons is responsible for the radial dependence of T_i/T_e, which is especially pronounced under sheath-limited and high-recycling conditions (Fig. 4.9a,b). Under detached conditions, radiative power losses reduce the electron temperatures below the ion temperatures, resulting in unequilibrated target plasmas (Fig. 4.9c).

The atom-only UEDGE simulations indicate thermal ion-electron equilibration to impact the effective H_2 dissociation rate under detached conditions only. However, the UEDGE simulations were performed using the

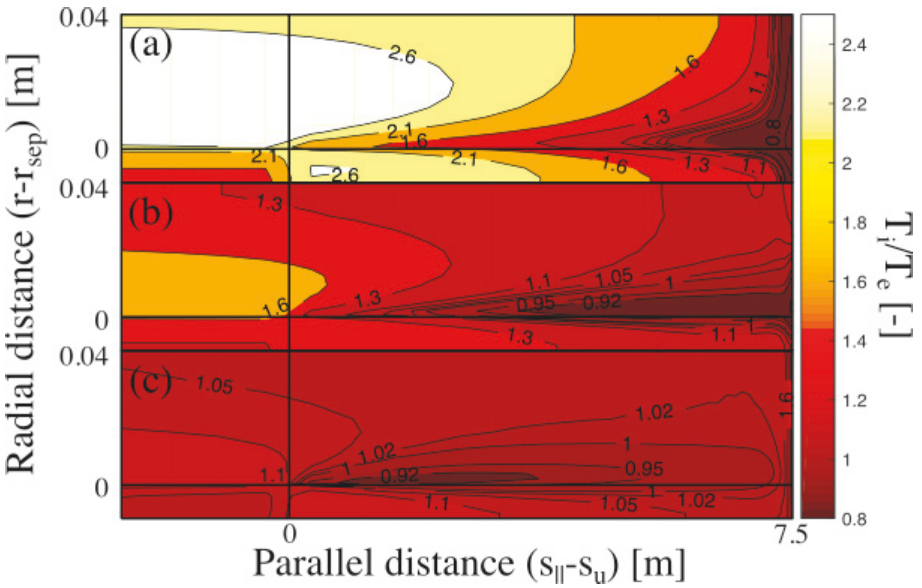

Figure 4.9. Surfaces for the degree of ion-electron thermal equilibration for sheath-limited (a), high-recycling (b), and detached (c) two-dimensional UEDGE simulations using the atom-only model. The X-point is located at $s_{||} - s_u = 0$ m and the target at $s_{||} - s_u = 7.5$ m. Adapted from Publication III.

atom-only model and do not self-consistently evaluate the effects of thermal ion-electron equilibration on the molecularly-induced plasma sinks and sources.

Impact of collisional-radiative processes on effective sinks and sources

EIRENE predictions using the metastable-resolved and metastable-unresolved models (Ch. 3.1) at quasi steady-state were compared to assess the role of different CR processes processes affecting H_2 depletion, as detailed in Publication IV. As the vibrational distribution is implicitly evaluated in the metastable-unresolved setup, it is not possible to directly compare the vibrational distribution. Instead, the effective dissociation rates are compared for the simulations. As all other reactions are identical between the models, any differences in the effective dissociation rates are caused by the different CR processes considered in the H_2 depletion rates.

The metastable-resolved effective dissociation rates are 25-60% lower compared to the metastable-unresolved rates in the molecular-relevant regime ($1\ \mathrm{eV} \lesssim \mathrm{T_e} \lesssim 5\ \mathrm{eV}$) due to differences between the CR processes for each of the H_2 depletion reactions (Fig. 4.10). The metastable-unresolved electron-impact ionization (EI) rates assume the molecules to be in their vibrational ground state and considers electronic transitions only. Replacing the metastable-resolved EI rates by the metastable-unresolved rates improves the agreement between the setups for all $T_e > 2$ eV, removing most of the systematic difference for $T_e > 8$ eV (Figure 4.10, red line).

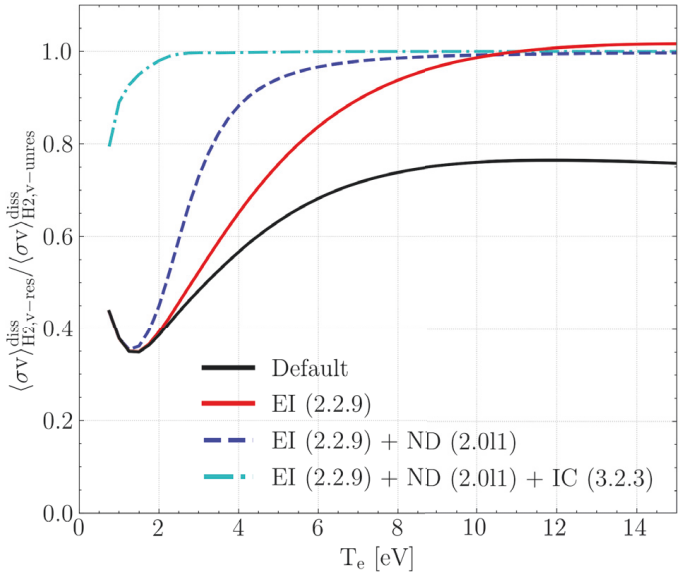

Figure 4.10. Ratio of the effective dissociation rates for the metastable-resolved EIRENE model to that of the metastable-unresolved EIRENE model as a function of plasma temperature shown for plasma density $n_e = 10 \times 10^{20}$ m^{-3}. The different lines represent the matching of the different rates, e.g. for the red line both the metastable-resolved and metastable-unresolved EIRENE simulations use the same EI rates, and for the cyan line only the DEA rates differ between the setups. Taken from Publication IV.

This increase in the effective dissociation rate is indicative of the role of electronic transitions for the EI channel in the ionization-dominated regime ($T_e \gtrsim 5$ eV). Removing the vibrational dependence and coupling to the electronically excited states from the neutral dissociation (ND) rates by using the vibrational ground state ND rates for both models further improves the agreement for $T_e > 1.5$ eV (Figure 4.10, blue line). The metastable-unresolved ND rates includes off-diagonal vibrational transitions ($v \rightarrow v \pm N,\ N \geq 1$) and coupling to excited electronic states, which are not considered by the metastable-resolved ND rates. Consequently, these processes are relevant for the ND channel for $1.5\ \text{eV} < \text{T}_\text{e} < 10\ \text{eV}$. Considering the full vibrational transition matrix in the vibrationally resolved ion conversion (IC) rates by using the metastable-unresolved IC rates in the metastable-resolved model improves the agreement between the setups for $T_e < 4$ eV (Figure 4.10, cyan line). This indicates that the role of off-diagonal vibrational transitions is significant for IC for $T_e < 4$ eV. The remaining difference between the metastable-resolved and unresolved effective dissociation rates for $T_e < 1.5$ eV (Figure 4.10, cyan line) is due to differences in the dissociative electron attachment (DEA) rates used by the setups. The metastable-unresolved DEA rates consider off-diagonal vibrational transitions that the metastable-resolved rates do not consider, that affect the effective dissociation rates via the DEA channel when $T_e < 1.5$ eV.

The differences in effective dissociation rates highlights the role CR processes when calculating the individual reaction rates. The metastable-unresolved rates did not, however, consider all possible CR processes, such as dependence on the test particle energy for IC or electronic transitions for DEA. Considering additional CR processes when calculating the metastable-unresolved effective rates is expected to further increase the difference to the metastable-resolved effective dissociation rates. The metastable-resolved rates are only available as H.2-type rates and are, thus, not coupled to the electronically excited states and only consider diagonal vibrational transitions. Consequently, the role of non-local transport effects cannot be evaluated without simultaneously considering the role of CR processes.

Approximating the H_2 vibrational equilibration mean-free path using EIRENE

Transport of vibrationally excited states results in non-local effects that are not considered by the CR models, which assume QSS locally. Non-local transport effects are relevant when the vibrational equilibration mean-free path ($\mathrm{P_{QSS}(v)}$) exceeds the spatial discretization of the numerical domain. Under such conditions the vibrationally-metastable states do not achieve $\mathrm{P_{QSS}(v)}$ and, subsequently, the vibrational molecular distribution is shifted towards the vibrational state of the molecular source [27, 60], which depends on surface effects [72].

Metastable-resolved EIRENE simulations, detailed in Publication IV, are performed for a simplified, Cartesian geometry with 100% absorbing boundaries to approximate $\mathrm{P_{QSS}(v)}$. The numerical domain has dimensions $\mathrm{L \times L}$ with a central $\mathrm{H_2}$ source and is assigned a constant plasma temperature and density. The temperature is varied in the interval 0.5 eV$< T_e <$15 eV for $n \in \{1 \times 10^{19}\ \mathrm{m^{-3}}, 1 \times 10^{20}\ \mathrm{m^{-3}}, 1 \times 10^{21}\ \mathrm{m^{-3}}\}$. Parameter scans are performed for domain dimensions $L \in \{0.5\ \mathrm{cm}, 1\ \mathrm{cm}, 5\ \mathrm{cm}, 20\ \mathrm{cm}\}$ and compared to the CR-predicted equilibrium vibrational distribution to obtain an approximation for the vibrational mean-free path, as described in Publication IV. When the QSS vibrational distribution is obtained by the metastable-resolved EIRENE simulations, half the cell side length $L/2$ is considered to be in excess of λ_{mfp}^{Peq}. Here, the fraction of molecules in their vibrational ground state is taken to be representative of QSS vibrational distribution.

The vibrational equilibration mean-free path is found to be $\lambda_{mfp}^{Peq} \gg 10\ \mathrm{cm}$, $\lambda_{mfp}^{Peq} \approx 10\ \mathrm{cm}$, and $\lambda_{mfp}^{Peq} \approx 2.5\ \mathrm{cm}$ for plasma background densities of $1 \times 10^{19}\ \mathrm{m^{-3}}$, $1 \times 10^{20}\ \mathrm{m^{-3}}$, and $1 \times 10^{21}\ \mathrm{m^{-3}}$, respectively (Fig. 4.11). Grids with sufficient resolution to resolve the plasma temperature and density gradients (typically order of millimeters) are necessary close to the target to reduce the discretization error. Thus, plasmas with densities below $n = 1 \times 10^{21}\ \mathrm{m^{-3}}$ are not expected to be vibrationally equilibrated close to

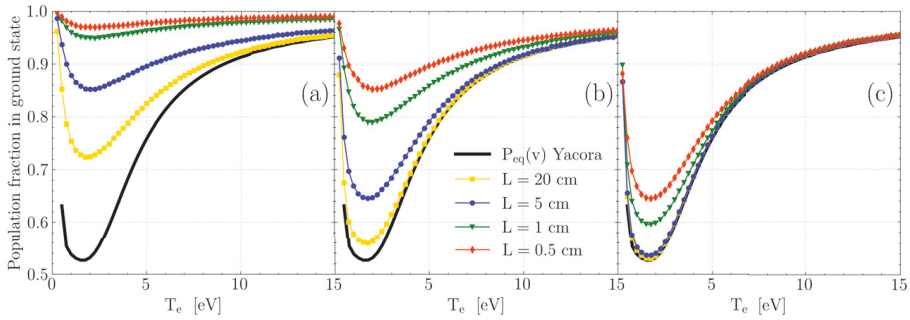

Figure 4.11. Population fraction in the vibrational H_2 ground state as a function of temperature for plasma density $n = 1 \times 10^{19}$ m^{-3} (a), $n = 1 \times 10^{20}$ m^{-3} (b), and $n = 1 \times 10^{21}$ m^{-3} (c) for varying cell side-length L. The vibrational equilibrium distribution $P_{QSS}(v)$ is calculated assuming local vibrational equilibrium. Taken from Publication IV.

the divertor targets. As plasma densities, even under detachment, typically are not expected to significantly exceed $n = 1 \times 10^{21}$ m^{-3}, transport of vibrational states is expected to impact the vibrational distribution and the effective molecular dissociation sink.

Estimation of non-local transport phenomena on effective sinks and sources using EIRENE

The effect of non-local transport on the effective dissociation rate, occurring when λ_{mfp}^{Peq} locally exceeds the spatial discretization, is evaluated for a one-dimensional flux-tube. EIRENE simulations of hydrogen plasmas, described in detail in Publication IV, are performed for a 3 m long, 112-cell flux-tube on static background plasmas generated by UEDGE-CRUMPET. The grid is concentrated at the target, where the cells have ~ 4 mm poloidal width.

The metastable-resolved EIRENE model predicts effective dissociation rates up to 30% and 50% lower than the metastable-unresolved setup in the ionization-dominated ($T_e > 10$) and molecular-relevant ($T_e \lesssim 5$ eV) regimes, respectively (Fig. 4.12). The metastable-unresolved EIRENE predictions show that the molecules do not reach the QSS vibrational equilibrium along the flux tube before being transported upstream and consequently dissociated. As the EIRENE predictions include both the net effect of transport of vibrational-metastable states and the impact of CR processes, the role of non-local transport effects cannot be distinguished from the effect of considering different CR processes. In the ionization-dominated regime ($T_e > 5$ eV), the 30% difference is due to different CR processes being considered by the metastable-resolved and unresolved simulations as dissociation is expected to be strong. Under detached conditions, λ_{mfp}^{Peq} significantly exceeds the poloidal cell widths (Fig. 4.11) and transport effects are, thus, expected to influence the effective dissociation rate. To assess the role of transport of metastable states on the effective dissociation

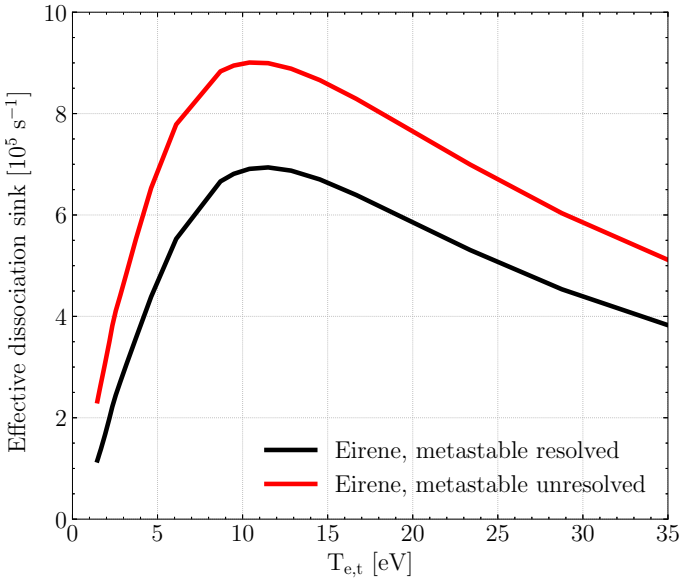

Figure 4.12. Effective dissociation sink for the metastable-unresolved (red) and metastable-resolved (black) EIRENE setups as a function of upstream electron temperature. The effective dissociation sink is taken as the integrated dissociation sink in the flux tube normalized to the molecular content. Adapted from Publication IV.

rate, reaction rates that consider the same CR processes for both the metastable-resolved and unresolved models are required.

4.4 Impact of the fluid molecular model on UEDGE simulations of experimental DIII-D deuterium L-mode plasmas

UEDGE simulations using the atom-only, DEID, and UEDGE-CRUMPET models are compared to DIII-D measurements of the ion saturation current, electron temperature, and electron density to assess the role of molecular processes on code-experiment agreement. The measurements, the atom-only, and the DEID model predictions are presented in Publication V. The simulations including drifts in Publication V are repeated using the UEDGE-CRUMPET model to assess the impact of considering CR processes in the UEDGE model. All UEGDE simulations were performed using the same radial transport coefficients to evaluate the impact of the molecular model independent of other parameters. The predicted plasma profiles display a strong dependency on the assumed radial transport coefficients [73]. Thus, the sensitivity of the UEDGE-predicted profiles on the assumed radial transport coefficients should be investigated to quantify the general dependence of UEDGE-experiment agreement on the choice of the radial transport coefficients. In addition, the atom-only simulations did not converge for LFS-midplane separatrix electron den-

sity $n_{e,sep}^{LFS-mp} < 1.7 \times 10^{19}$ in the studies presented in Publication V. The cause of this behavior was not identified, but is likely linked to numerical boundary condition instabilities when drifts are included, which are relaxed by the introduction of a third hydrogenic species. The case was eventually abandoned in favor of development of the fluid molecular model, but should be revisited in subsequent works. As discussed in section 1.2, the CR modeling was performed using hydrogen data, which should be observed when interpreting the results herein.

UEDGE predicts a peak target density ($n_{e,peak}^{LFS-t}$) roll-over qualitatively different from the measurements, and the simulations under-estimate the LFS target peak saturation current ($J_{sat,peak}^{LFS-t}$) and $n_{e,peak}^{LFS-t}$ compared to the measurements (Fig. 4.13a,c). Accounting for the different parallel locations of the DTS chord used for $n_{e,peak}^{LFS-t}$ measurements compared to the target profiles used in UEDGE does not improve the code-experiment agreement. The under-estimation is observed for all analyzed UEDGE models and for other plasma-edge codes that are coupled to EIRENE [64]. Hence, the under-estimation is assumed to be caused by discrepancies in the plasma model, likely associated with the treatment of the boundary conditions and plasma transport model, rather than to be caused by the atomic or molecular processes or model. Further investigations of this discrepancy are, however, outside the scope of this dissertation. Consequently, the qualitative code-experiment agreement and the quantitative effects of molecular processes relative to the atom-only model are assessed herein.

Including vibrational and electronic ground state molecules as a separate fluid species in UEDGE is necessary to qualitative achieve the measured $J_{sat,peak}^{LFS-t}$ roll-over (Fig. 4.13). The roll-over of $J_{sat,peak}^{LFS-t}$ is caused by the increased effective ionization mean-free path of the recycled molecules predicted by the DEID model and by the collisional-radiative, molecularly-induced plasma particle and power sinks considered in the UEDGE-CRUMPET model.

The longer effective ionization mean-free paths of the recycled molecules predicted by the DEID model, compared to the atom-only model, results in the ionization front situating further poloidally upstream from the target compared to the atom-only predictions. As $n_{e,sep}^{LFS-mp}$ increases, the ionization front moves poloidally upstream towards the X-point, which decreases $n_{e,peak}^{LFS-t}$ compared to the atom-only simulations under high-recycling conditions (Fig. 4.13c). This observation is consistent with the DEID and atom-only predictions in section 4.1. At sufficiently high $n_{e,sep}^{LFS-mp}$, the increased effective ionization mean-free paths of the recycled molecules, combined with the cross-field drifts reducing the HFS divertor plasma temperatures, causes the HFS ionization front to enter the core region. As the ionization front enters the core region a stable X-point MARFE [74] forms, resulting in radiative power exhaust in the core, which decreases the divertor power and detaches the LFS target (Fig. 4.13a). Neither an

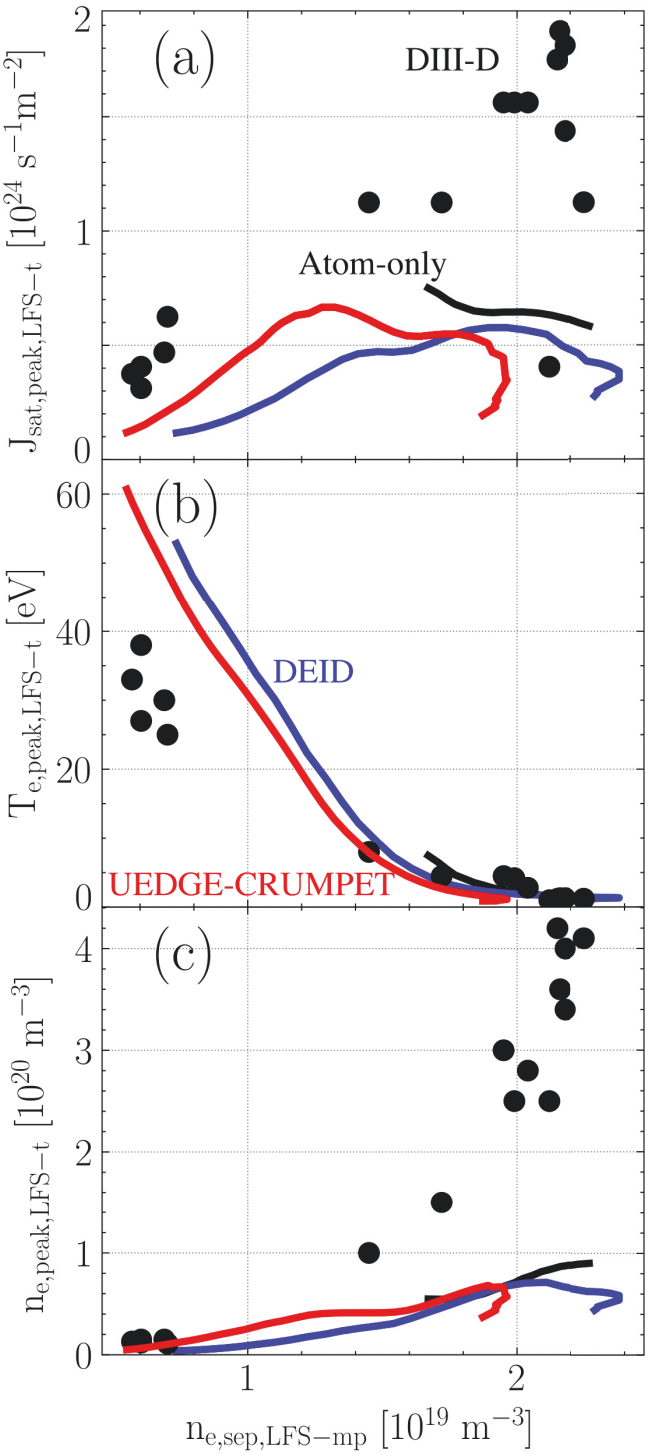

Figure 4.13. Measured DIII–D (circles) LFS peak target saturation current (a), electron temperature (b), and density (c) together with the UEDGE predictions using the UEDGE-CRUMPET (red), DEID (blue) and atom-only (black) models as a function of LFS electron separatrix density. Adapted from Publication V.

X-point MARFE nor a roll-over in $n_{e,peak}^{LFS-t}$ are experimentally observed within the range of plasma densities investigated. This indicates that the observed detachment due to the increased effective ionization mean-free paths predicted by the DEID model compared to the atom-only model does not correspond to the experimentally observed behavior.

The molecularly-induced plasma power and particle sinks considered by the UEDGE-CRUMPET model, discussed in Section 4.1, results in $J_{sat,peak}^{LFS-t}$ and $n_{e,peak}^{LFS-t}$ saturating and decreasing with increasing $n_{e,sep}LFS-mp$ (Fig. 4.13a,c). The molecularly-induced plasma power sinks increases the net power losses, reducing $T_{e,peak}^{LFS-t}$, for the same $n_{e,sep}^{LFS-mp}$ compared to the DEID and atom-only models (Fig. 4.14 and 4.13b). With increasing $n_{e,sep}^{LFS-mp}$, the power losses increase (Fig. 4.14) and $T_{e,peak}^{LFS-t}$ decreases until MAR processes occur in the divertor and detachment is achieved. Further increasing $n_{e,sep}^{LFS-mp}$ results in an unstable X-point MARFE forming, disrupting the plasma simulation within a short core electron density interval, which is the independent parameter in the UEDGE simulations.

Including molecules as a separate fluid species shifts the DEID and UEDGE-CRUMPET predicted $T_{e,peak}^{LFS-t}$ profiles to 10% and 15% lower $n_{e,sep}^{LFS-mp}$ compared to the atom-only predictions, respectively (Fig. 4.13b). The corresponding shift is also observed for the $J_{sat,peak}^{LFS-t}$ and $n_{e,peak}^{LFS-t}$ predictions (Fig. 4.13a,c). The decrease in $T_{e,peak}^{LFS-t}$ for the same $n_{e,sep}^{LFS-mp}$ is indicative of increased power losses along the SOL compared to the atom-only model. The additional SOL plasma power losses are due to ion-molecule thermal equipartition in the DEID model, which does not consider molecularly-induced plasma power sinks and over-estimates the molecular densities due to low dissociation rates (Sec. 4.1). The UEDGE-CRUMPET model considers molecularly-induced power sinks that increase the radiated power in the SOL (Fig. 4.14). As the shift in $T_{e,peak}^{LFS-t}$ profiles predicted by the UEDGE-CRUMPET model is larger than that predicted by the DEID model, the molecularly-induced plasma power sinks are stronger than the ion-molecule thermal equipartition power sink.

The molecularly-induced plasma power sink (P_{H_2}), dominated by binding energy, considered by the UEDGE-CRUMPET model increases the net radiative plasma power loss ($P_{H_2} + P_{rad} + P_Z$) for $n_{e,sep}^{LFS-mp} < 1.5 \times 10^{19}$ m^{-3} compared to the DEID predictions (Fig. 4.14). The UEDGE-CRUMPET model predicts a plateau in hydrogen atomic (Lyman and Balmer series) and molecular (Lyman-Werner) radiated power ($P_{H_2} + P_{rad}$) for 1.3×10^{19} m^{-3} $< \mathrm{n}_{\mathrm{e,sep}}^{\mathrm{LFS-mp}} <$ 1.8×10^{19} m^{-3} not observed in the DEID predictions (Fig. 4.14). The net radiative plasma power losses are sustained by an increase in carbon impurity radiation, due to intrinsic carbon sputtering, in the UEDGE-CRUMPET model. The onset of detachment is mediated by a strong increase in the carbon radiated power exhausting the plasma power observed in the UEDGE-CRUMPET and DEID simulations, but not in the atom-only simulations (Fig. 4.14). The observed increase of

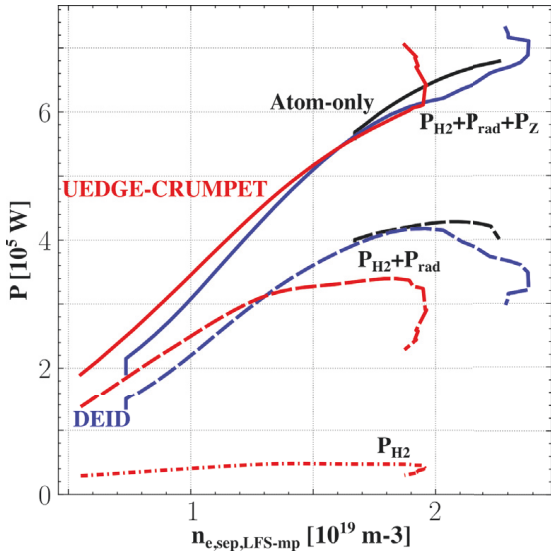

Figure 4.14. UEDGE-predicted volumetric plasma power losses for the atom-only (black), DEID (blue), and UEDGE-CRUMPET (red) simulations as a function of LFS-MP electron density. Here, P_{H_2} are the molecularly-induced plasma power losses to binding energy and radiation, P_{rad} the radiative power losses from hydrogenic atoms, and P_Z the impurity radiation power losses. Adapted from Publication V.

carbon impurity radiation and onset of detachment when molecules are included in the UEDGE simulations indicate an indirect dependence of carbon impurity sputtering and transport on molecular effects in UEDGE (Figs. 4.14 and 4.13a). The UEDGE carbon transport and sputtering models are not explicitly dependent on molecules. Thus, any differences in carbon carbon radiation are due to an implicit dependence on molecular processes via ion, electron, and atom temperatures, densities, and flows.

The molecular self-collisional mean-free path at onset of detachment as predicted by the UEDGE-CRUMPET model is $\lambda_{mfp}^{H_2-H_2} \approx 0.2$ m. Assuming $L = 1$ m, as the molecules are not bound by the magnetic field lines and only limited by the device size, the molecular self-collisionality is $\nu_{H_2}^* = 5 - 10$ under detached conditions (Eq. 1.11). The increase in $\nu_{H_2}^*$ compared to that in Ch. 4.2 is due to the closed domain, resulting in weaker particle pumping and higher molecular densities. The molecular elastic self-scattering rate is the same as in Ch. 4.2 ($K_{el}^{H_2-H_2} = 5 \times 10^{-16}$ m^{3}s$^{-1} \ll \langle \sigma v \rangle_{diss}$). Thus, the molecules predominantly dissociate rather than scatter elastically. Adapting a temperature-dependent elastic scattering rate in UEDGE is expected to make the molecules collisional ($\nu_{H_2}^* \gg 1$) under molecular-relevant conditions (1 eV $\lesssim T_e \lesssim$ 5 eV), which justifies a fluid treatment of the molecules. However, fluid predictions of the molecular density and energy under non-collisional conditions were within 15% and a factor of 2 of kinetic EIRENE predictions without molecular self-scattering, respectively (Ch. 4.2). This analysis indicates a limited impact of non-Maxwellian

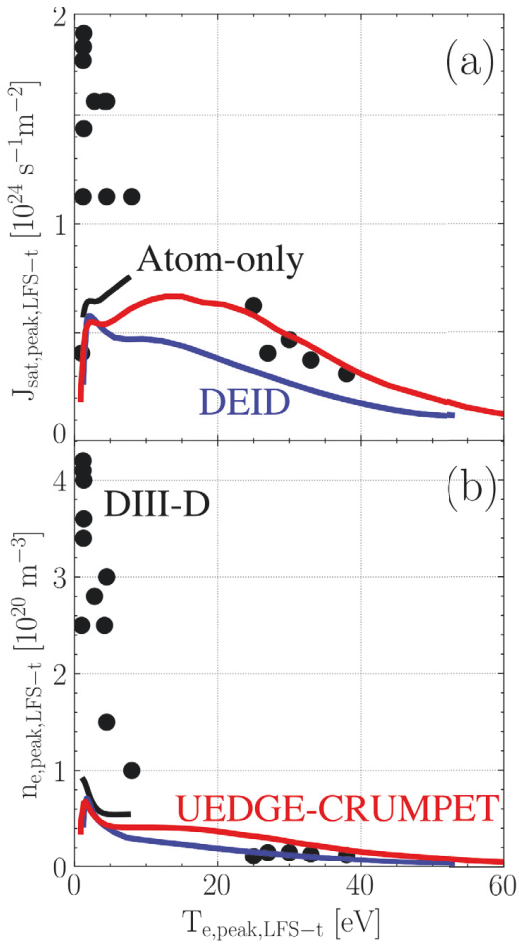

Figure 4.15. Measured DIII–D (circles) LFS peak target saturation current (a) and density (b) together with the UEDGE predictions using the UEDGE-CRUMPET (red), DEID (blue), and atom-only (black) models as a function of LFS target peak electron temperature. Adapted from Publication V.

effects on the UEDGE predictions.

Divertor detachment is a local divertor phenomenon, driven by target recycling and the local divertor conditions. Consequently, the capability of the different UEDGE models to capture detachment are evaluated by considering the target plasma conditions as a function of $T_{e,peak}^{LFS-t}$.

The UEDGE-CRUMPET model predicts local $J_{sat,peak}^{LFS-t}$-profiles in quantitative agreement with the probe measurements for $T_e > 20$ eV, when the DEID model under-predicts $J_{sat,peak}^{LFS-t}$ (Fig. 4.15a). This behavior is indicative of the molecular processes considered by the models affecting the local divertor conditions outside the molecular-relevant regime ($1\text{ eV} \lesssim T_e \lesssim 5\text{ eV}$), for which the difference in the dissociation rates are sufficiently large. For reference, the DEID dissociation rate at 40 eV correspond to the DEID dissociation rate at 6 eV, whereas the UEDGE-CRUMPET dissociation rate at 40 eV is a factor of 50 higher than the DEID rate (Sec. 4.1).

The UEDGE-CRUMPET predictions are qualitatively different from the probe-measured $J_{sat,peak}^{LFS-t}$ for $1.5\ \mathrm{eV} \lesssim T_e \lesssim 15\ \mathrm{eV}$ (Fig. 4.15a). This qualitative difference is likely an effect of the under-estimation of $J_{sat,peak}^{LFS-t}$ and $n_{e,peak}^{LFS-t}$ compared to the DTS measurements for $T_e < 10\ \mathrm{eV}$. As discussed above, the under-estimation is assumed to be due to the plasma boundary conditions and radial transport model affecting the plasma predictions, as the same effect is observed for all UEDGE models and other plasma-edge codes [64]. Relaxing the plasma boundary conditions, and implementing a more physics-based radial transport model, to better match the plasma measurements is likely to improve the qualitative and quantitative agreement of the UEDGE-CRUMPET model with the probe-measured $J_{sat,peak}^{LFS-t}$ for $1.5\ \mathrm{eV} \lesssim T_e \lesssim 15\ \mathrm{eV}$.

The UEDGE-CRUMPET and DEID $n_{e,peak}^{LFS-t}$ predictions are qualitatively similar to one another, but qualitatively different from the atom-only predictions (Fig. 4.15b). This behavior indicates the local effects of considering MAR processes are similar to the increase in effective ionization mean-free paths of the molecules considered by the UEDGE-CRUMPET and DEID models, respectively. Both aforementioned processes reduce the plasma densities at the target under low-temperature conditions ($T_e < 1.5\ \mathrm{eV}$). There is, however, no physics justification for the strong increase of the effective ionization mean-free paths predicted by the DEID model compared to the atom-only or UEDGE-CRUMPET predictions. The plasma power losses in the atom-only model are insufficient to reduce T_e to the sub-eV temperature range for which EIR reduces the target plasma densities.

The UEDGE simulations analyzed herein assume the maximum possible role of molecular effects on the plasma as all target fluxes are recycled as thermal molecules. This results in an over-estimation of molecular processes in the DEID and UEDGE-CRUMPET models compared to the DIII-D measurements, for which the molecular recycling of up to 90% is expected. The atom-only simulations represent 0% molecular recycling, which is the opposite extreme. Thus, the effect of varying the fraction of molecular recycling assumed in the UEDGE-CRUMPET and DEID simulations is limited by the atom-only prediction. Consequently, the quantitative agreement between the UEDGE predictions and the DIII-D measurements is independent of the molecular recycling fraction.

5. Summary and outlook

Understanding the physics of divertor detachment onset and its formation is crucial for the design of future fusion power plants. Fusion reactors are foreseen to operate under detached conditions to limit the power loads reaching the reactor plasma-facing components within their thermomechanical properties. Detachment is a local divertor phenomenon driven by plasma recycling at the divertor targets and the local divertor conditions. Therefore, divertor detachment is affected by molecular processes, which are expected to be significant under detachment-relevant plasma temperatures ($1\ \mathrm{eV} \lesssim \mathrm{T_e} \lesssim 5\ \mathrm{eV}$). This dissertation evaluates the role of molecular processes in producing divertor detachment using a collisional-radiative fluid model for molecules implemented in the edge-fluid code UEDGE, the kinetic molecular model in EIRENE, and experimental DIII-D deuterium plasmas in low-confinement mode (L-mode).

UEDGE simulations considering fluid hydrogen molecules indicate molecular effects are necessary to produce divertor detachment in a one-dimensional computational domain. Collisional-radiative (CR), molecularly-induced plasma power sinks reduce the plasma target temperatures sufficiently for molecularly-assisted recombination (MAR) and electron-ion recombination (EIR) to occur in the divertor volume. When molecularly-induced plasma power losses and MAR are omitted, the plasma temperatures are too high for EIR recombination, occurring at lower electron temperature ($T_e \lesssim 1\ \mathrm{eV}$) than MAR ($T_e \lesssim 2\ \mathrm{eV}$), to detach the divertor plasma.

Presently, the UEDGE fluid model for molecules assumes negligible molecular velocities, and the molecular diffusive momentum equation is not coupled to the ion and atom momentum equations. As the plasma momentum losses contribute to divertor detachment, ion-molecule scattering is expected to affect the onset of plasma detachment. Therefore, the molecular model in UEDGE needs to be updated to consider the plasma momentum sink due to ion-molecule friction. The UEDGE recycling model assumes the molecules to be released as electronic and vibrational ground state molecules. Accounting for preferential release as vibrationally ex-

cited molecules depending on a surface model is expected to affect the molecularly-induced plasma particle and energy sinks and sources.

Comparisons of UEDGE and EIRENE predictions show that the applicability of the molecular fluid model is affected by kinetic transport effects when $\mathbf{T_e \lesssim 5}$ eV. The diffusive UEDGE fluid molecular model over-estimates the molecular content and mean energy by approximately 15% and a factor of 2, respectively, compared to the EIRENE kinetic molecular model for $T_e \lesssim 5$ eV. For $T_e > 5$ eV the different treatment of CR processes in the UEDGE and EIRENE models is dominant. The UEDGE-predicted mean molecular energy displays a negligible dependence on the CR processes considered by the model.

The EIRENE setup evaluated in this work does not include neutral-neutral (atom-atom, atom-molecule, and molecule-molecule) interactions, which are inherently considered by the UEDGE fluid model. Including neutral-neutral interactions in EIRENE is expected to alleviate the differences between the fluid and kinetic molecular models. Additionally, the UEDGE model currently assumes constant ion-molecule and atom-molecule scattering rates, whereas EIRENE evaluates temperature-dependent elastic scattering rates. Including the corresponding temperature-dependent elastic scattering rates in the UEDGE molecular model is expected to improve the UEDGE-EIRENE agreement.

The role of CR processes considered is found to be more significant than the role of vibrational transport and assuming ion-electron thermal equilibrium. The EIRENE-predicted effective dissociation rate decreased by up to 65% when vibrational and electronic transitions were omitted from the CR model compared to when they were included. Comparison of EIRENE simulations to CR-calculated equilibrium vibrational distributions found the vibrational equilibration mean-free paths for hydrogen molecules to be in excess of 2.5 cm for local plasma densities below 1×10^{21} m^{-3} at $T_e = 2$ eV. Consequently, the molecular vibrational equilibration mean-free paths exceeds the typical poloidal length of the computational grid cells at the target and non-local transport effects are expected to affect the effective molecular dissociation rates. The degree of ion-electron thermal equilibration was found to affect the effective CR dissociation rates for $T_e \lesssim 3$ eV. UEDGE simulations predict ion-electron thermal equilibration to affect the effective dissociation rate ($T_e \neq T_i$ and $T_e < 3$ eV) for detached divertor conditions only.

Molecular reaction rates for the vibrationally resolved simulations that considered the same CR processes as the vibrationally unresolved rates are currently not available in the EIRENE molecular reaction databases. Hence, the role of non-local transport effects could not be assessed independently from the effect of electronic and vibrational CR transitions using EIRENE. By incorporating a CR model in the transport code, so that full CR system can be evaluated self-consistently for each cell in the

simulation domain, non-local transport and CR effects could be evaluated independently.

Including fluid molecules in UEDGE simulations of DIII-D deuterium plasmas in L-mode like conditions improves the qualitative code-experiment agreement at the onset of detachment compared to UEDGE simulations considering atoms only. An increase in carbon impurity radiation along the scrape-off layer (SOL) is predicted by UEDGE at the onset of detachment when molecules are included in the simulations. This increase is indicative of molecular processes indirectly affecting the UEDGE-predicted carbon impurity transport and sputtering via the ion, electron, and atom temperatures, densities, and flows. The effect of molecular processes on the plasma power losses along the SOL are expected to be small compared to the effect of radial transport coefficients on the plasma power losses along the SOL. Therefore, the radial transport coefficients need to be varied in future simulations to assess the sensitivity of the UEDGE predictions on radial transport. When the onset of detachment is evaluated as a function of the local divertor temperature, the molecularly-induced plasma particle and power sinks improve the qualitative agreement of the predicted onset of detachment with DIII-D measurements compared to the atom-only simulations. The quantitative code-experiment agreement is, however, not improved and the discrepancy is assumed to stem in the applied plasma boundary conditions and radial transport model. Relaxing the plasma boundary conditions and matching the radial transport to the experiments is expected to improve both the qualitative and quantitative agreement of the UEDGE simulations with the experimental DIII-D plasmas when molecules are included as a separate species.

The CR effective rates employed by the UEDGE fluid model for molecules are calculated assuming hydrogen molecules, independent of the molecular isotopologue (H_2, D_2, T_2, HT, or DT) used in the UEDGE transport simulations. Consequently, the simulations of the DIII-D deuterium plasmas evaluate the transport of D_2 using H_2 dissociation rates. The corresponding CR system of equations needs to be constructed individually for each isotopologue to be simulated and the CR effective reactions calculated to ensure self-consistent treatment of the hydrogenic isotopologues.

The presently implemented UEDGE recycling model considers a user-defined molecular recycling fraction only. The diffusion-driven molecular transport assumed in UEDGE does not accurately capture the effects of recycling when radial plasma gradients are negligible, as shown in Publication I. Thus, the recycling model in UEDGE could be refined by considering surface recycling databases and formulating recycling boundary conditions for fluid models that consider a velocity distribution for individual molecules.

References

[1] J. Wesson and D. J. Campbell, *Tokamaks*. 4th Edition. Oxford University Press, 2011. ISBN: 978-0-19-959223-4.

[2] Y. Kamada et al., *Fusion Science and Technology* **42** (2002) 185.

[3] Y. Shimomura et al., *Nuclear Fusion* **39** (1999) 1295.

[4] K. Ikeda, *Nuclear Fusion* **47** (2007).

[5] E. J. Doyle et al., *Nuclear Fusion* **47** (2007) S18.

[6] A. V. Chankin, *Journal of Nuclear Materials* **241** (1997) 199.

[7] A. V. Chankin et al., *Plasma Physics and Controlled Fusion* **57** (2015) 095002.

[8] V. A. Vershkov and C. A. V. *Sovjet Journal of Plasma Physics* **14** (1989) 371.

[9] P. C. Stangeby, *The plasma boundary of magnetic fusion devices*. Bristol and Philadelphia: IoP Publishing, 2000. ISBN: 0-7503-0559-2.

[10] D. Bohm, *The characteristics of electrical discharges in magnetic fields*. New York: McGraw-Hill, 1949.

[11] R. Chodura, "Plasma flow in the sheath and the presheath of a scrape-off layer". In: *Post D.E., Behrisch R. (eds) Physics of plasma-wall interactions in controlled fusion*. Boston: Springer, 1986. ISBN: 978-1-4757-0069-5.

[12] J. G. Watkins et al., *Review of Scientific Instruments* **92** (2021) 053523.

[13] S. Brezinsek et al., *Plasma Physics and Controlled Fusion* **47** (2005) 615.

[14] J. L. Luxon, *Nuclear Fusion* **42** (2002) 614.

[15] M. Keilhacker et al., *Nuclear Fusion* **39** (1999) 209.

[16] A. E. Järvinen et al., *Proceedings of the 40th EPS Conference on Plasma Physics*. 1 July to 5 July 2013, Espoo, Finland.

[17] A. E. Jaervinen et al., *Nuclear Fusion* **56** (2016) 046012.

[18] G. Sergienko et al., *Journal of Nuclear Materials* **438** (2013) S1100.

[19] T. Donné et al., *European Research Roadmap to the Realisation of Fusion Energy*. Garching: EUROfusion, Programme Management Unit, 2018. ISBN: 978-3-00-061152-0.

[20] H. Zohm et al., *Nuclear Fusion* **53** (2013) 073019.

[21] G. Federici et al., *Fusion Engineering and Design* **109** (2016) 1464.

[22] C. Guillemaut et al., *Nuclear Fusion* **45** (2014) 093012.

[23] A. Yu. Pigarov and S. I. Krasheninnikov, *Physics Letters A* **222** (1996) 251.

[24] S. I. Krasheninnikov et al., *Physics Letters A* **214** (1996) 285.

[25] S. I. Krasheninnikov, *Physica Scripta* **T96** (2002) 7.

[26] A. S. Kukushkin et al., *Nuclear Materials and Energy* **12** (2017) 984.

[27] U. Fantz et al., *Journal of Nuclear Materials* **290** (2001) 367.

[28] E. U. Condon, *American journal of physics* **15** (1947) 365.

[29] R. K. Janev et al., *Elementary Processes in Hydrogen-Helium Plasmas*. Berlin: Springer-Verlag, 1987. ISBN: 978-3-642-71937-0.

[30] M. Blommaert et al., *Nuclear Materials and Energy* **19** (2019) 28.

[31] W. Van Uytven et al., *Contributions to Plasma Physics* (2022) e202100191.

[32] N. Horsten et al., *Contributions to Plasma Physics* **60** (2020) e201900132.

[33] N. Horsten et al., *Contributions to Plasma Physics* **58** (2018) 703.

[34] T. D. Rognlien et al., *Users Manual for the UEDGE Edge-Plasma Transport Code*. `https://github.com/LLNL/UEDGE`. [Online; accessed 23-September-2021].

[35] D. Reiter, *The EIRENE Code User Manual Including: B2-EIRENE Interface*. `http://www.eirene.de/eirene.pdf`. [Online; accessed 17-January-2022].

[36] D. R. Bates et al., *Proceedings of the Royal Society of London. Series A. Mathematical and Physical Sciences* **267** (1962) 297.

[37] R. McWhirter and A. Hearn, *Proceedings of the Physical Society (1958-1967)* **82** (1963) 641.

[38] P. T. Greenland, *Proceedings of the Royal Society of London* **457** (2001) 1821.

[39] P. T. Greenland, *The CRMOL Manual: Collisional-Radiative Models for Molecular Hydrogen in Plasmas*. Jülich: Forschungszentrum Jülich, Zentralbibliothek, 2001.

[40] P. T. Greenland et al., *The role of Molecular Hydrogen in Plasma Recombination*. Jülich: Forschungszentrum Jülich, Zentralbibliothek, 1996.

[41] T. Fujimoto and K. Sawada, *J. Appl. Phys* **78** (1995) 2913.

[42] K. Sawada and M. Goto, *Atoms* **4** (2016) 29.

[43] D. Wünderlich, "Berechnung von Teilchendichten für die Diagnostik an Niedertemperaturplasmen". PhD thesis. Mathematisch–Naturwissenschaftlichen Fakultät der Universität Augsburg, Sept. 2004.

[44] U. Fantz, "Molecular Diagnostics of Cold Edge Plasmas". In: *Clark R.E., Reiter D.H. (eds) Nuclear Fusion Research*. Berlin: Springer-Verlag, 2005. ISBN: 978-3-540-23038-0.

[45] R. K. Janev et al., *Collision Processes in Low-Temperature Hydrogen Plasmas*. Jülich: Forschungszentrum Jülich, Zentralbibliothek, 2003.

[46] C. S. Wang Chang and G. Uhlenbeck, *Transport Phenomena in Polyatomic Gases*. Ann Arbor: Engineering Research Institute, University of Michigan, 1951.

[47] R. Yano et al., *Physics of Fluids* **19** (2007) 017103.

[48] G. Bateman, *Distribution of neutrals scattered off a wall*. Princeton: PPPL Applied Physics Division, 1980.

[49] W. Eckstein and D. B. Heifetz, *Journal of Nuclear Materials* **145** (1987) 332.

[50] T. D. Rognlien et al., *Fusion Engineering and Design* **135** (2018) 380.

[51] D. Reiter, *The data file HYDHEL: Atomic and Molecular Data for EIRENE based upon: Janev, Langer, Evans, Post, "Elementary Processes in Hydrogen-Helium Plasmas", Springer 1987*. `http://eirene.de/hydhel.pdf`. [Online; accessed 23-September-2021].

[52] D. Reiter, *The data file H2VIBR: Additional Molecular Data for EIRENE: Vibrationally Resolved $H_2(X)$ Ground State*. `http://eirene.de/h2vibr.pdf`. [Online; accessed 23-September-2021].

[53] D. Reiter, *The Data File AMJUEL: Additional Atomic and Molecular Data for EIRENE*. `http://eirene.de/amjuel.pdf`. [Online; accessed 23-September-2021].

[54] D. Wünderlich et al., *Journal of Quantitative Spectroscopy and Radiative Transfer* **110** (2009) 62.

[55] D. Wünderlich et al., *Journal of Quantitative Spectroscopy and Radiative Transfer* **240** (2020) 106695.

[56] V. Kotov et al., *Plasma Physics and Controlled Fusion* **50** (2008) 105012.

[57] M. Wischmeier et al., *Contributions to Plasma Physics* **48** (2008) 249.

[58] H. P. Summers and M. G. O'Mullane, *Proceedings of the 17th International Conference on Atomic Processes in Plasmas*. 19 July to 22 July 2011, Belfast, Nothern Ireland, UK.

[59] H. P. Summers, *The ADAS User Manual v2.6 (2004)*. `https://www.adas.ac.uk/manual.php`. [Online; accessed 22-February-2022].

[60] K. Miyamoto et al., *Journal of Applied Physics* **93** (2003) 845.

[61] A. Holm, *CRUMPET: Collisional-Radiative UEDGE Model for Plasma Edge Theory*. https://github.com/holm10/CRUMPET. [Online; accessed 17-January-2022].

[62] R. K. Janev and J. J. Smith, "Cross Sections for Collision Processes of Hydrogen Atoms with Electrons, Protons and Multiply Charged Ions". In: *Bobeldijk C., Janev R. K. (eds) Atomic and Plasma-Material Interaction Data for Fusion. Vol 4*. Vienna: International Atomic Energy Agency, 1993.

[63] L. C. Johnson, *The Astrophysical Journal* **174** (1972) 227.

[64] M. Groth et al., *Nuclear Materials and Energy* **19** (2019) 211.

[65] A. E. Jaervinen et al., *Nuclear Materials and Energy* **12** (2017) 1136.

[66] G. D. Porter et al., *Physics of Plasmas* **7** (2000) 3663.

[67] A. V. Chankin et al., *Plasma Physics and Controlled Fusion* **57** (2015) 095002.

[68] N. H. Brooks et al., *Review of Scientific Instruments* **63** (1992) 5167.

[69] F. Glass et al., *Review of Scientific Instruments* **87** (2016) 11E508.

[70] A. W. Leonard et al., *Nuclear Fusion* **57** (2017) 086033.

[71] L. L. Lao et al., *Nuclear Fusion* **25** (1985) 1611.

[72] S. Saito et al., *Contributions to Plasma Physics* **60** (2020) e201900152.

[73] A. Zito et al., *Plasma Physics and Controlled Fusion* **63** (2021) 075003.

[74] B. Lipschultz, *Journal of Nuclear Materials* **145** (1987) 15.

Aalto-DT 106/2022

ISBN 978-952-64-0889-7 (printed)
ISBN 978-952-64-0890-3 (pdf)
ISSN 1799-4934 (printed)
ISSN 1799-4942 (pdf)

Aalto University
School of Science
Department of Applied Physics
www.aalto.fi

BUSINESS + ECONOMY

ART + DESIGN + ARCHITECTURE

SCIENCE + TECHNOLOGY

CROSSOVER

DOCTORAL THESES